

ISVR Technical Memorandum

SCIENTIFIC PUBLICATIONS BY THE ISVR

Technical Reports are published to promote timely dissemination of research results by ISVR personnel. This medium permits more detailed presentation than is usually acceptable for scientific journals. Responsibility for both the content and any opinions expressed rests entirely with the author(s).

Technical Memoranda are produced to enable the early or preliminary release of information by ISVR personnel where such release is deemed to be appropriate. Information contained in these memoranda may be incomplete, or form part of a continuing programme; this should be borne in mind when using or quoting from these documents.

Contract Reports are produced to record the results of scientific work carried out for sponsors, under contract. The ISVR treats these reports as confidential to sponsors and does not make them available for general circulation. Individual sponsors may, however, authorize subsequent release of the material.

COPYRIGHT NOTICE

(c) ISVR University of Southampton All rights reserved.

ISVR authorises you to view and download the Materials at this Web site ("Site") only for your personal, non-commercial use. This authorization is not a transfer of title in the Materials and copies of the Materials and is subject to the following restrictions: 1) you must retain, on all copies of the Materials downloaded, all copyright and other proprietary notices contained in the Materials; 2) you may not modify the Materials in any way or reproduce or publicly display, perform, or distribute or otherwise use them for any public or commercial purpose; and 3) you must not transfer the Materials to any other person unless you give them notice of, and they agree to accept, the obligations arising under these terms and conditions of use. You agree to abide by all additional restrictions displayed on the Site as it may be updated from time to time. This Site, including all Materials, is protected by worldwide copyright laws and treaty provisions. You agree to comply with all copyright laws worldwide in your use of this Site and to prevent any unauthorised copying of the Materials.

UNIVERSITY OF SOUTHAMPTON
INSTITUTE OF SOUND AND VIBRATION RESEARCH
DYNAMICS GROUP

A Multipoint Constraint Model for the Vibration of Spot Welded Structures

by

R.O. De Alba, N.S. Ferguson and B.R. Mace

ISVR Technical Memorandum No: 982

June 2009

Authorised for issue by
Professor Michael Brennan
Group Chairman

© Institute of Sound & Vibration Research

ABSTRACT

To evaluate the vibrational behaviour of spot welded structures, finite element (FE) models can be used. In modelling the structure, a model of the spot weld which is connected to the substructures by multipoint constraints (MPCs) has clear advantages. It can be located anywhere in the model and it is not necessary to re-mesh surfaces to assemble them together. However, analytical validation is needed. In this paper the results from FE models with MPCs are compared to analytical solutions to evaluate the accuracy of these connections and to analyze the influence of the size and the type of element for which these MPCs are applied. Two different models are analyzed: two infinite beams and two simply supported plates. In all models there is a single elastic connection with translational and rotational stiffnesses. Finally, component mode synthesis (CMS) is used in combination with an MPC spot weld model in order to reduce the size of the model and to facilitate the assembly of components. The results show that the MPC connection is not accurate when thin plate elements are used, due to the non-conforming formulation. In contrast, when a heterosis element was used the results show that the MPC connection is as accurate as a node-to-node connection. Finally, it is seen that when the MPC models are used in combination with CMS, the response of the system can be evaluated for any spot weld location in an accurate and numerically efficient manner.

CONTENTS

1	INTRODUCTION.....	1
2	SPOT WELD FINITE ELEMENT MODELS.....	3
2.1	Single beam models	3
2.2	Single Brick model.....	4
2.3	Area Contact Model 2	4
2.4	CWELD.....	4
2.5	Summary.....	6
3	MPC ELASTIC CONNECTION	7
4	VALIDATION OF A MULTIPOINT CONSTRAINT SPOT-WELD MODEL FOR ONE DIMENSIONAL SYSTEMS.....	9
4.1	Finite Element models.....	9
4.1.1	<i>Node to node connection.....</i>	<i>11</i>
4.1.2	<i>MPC connection.....</i>	<i>12</i>
4.2	Analytical solution.....	13
4.3	Numerical examples.....	13
4.3.1	<i>Accuracy of FE models: a single translational spring connection.....</i>	<i>15</i>
4.3.2	<i>Accuracy of FE models: a single rotational spring connection.....</i>	<i>15</i>

5	VALIDATION OF A MULTIPOINT CONSTRAINT SPOT-WELD MODEL FOR TWO DIMENSIONAL SYSTEMS.....	18
5.1	Finite element models.....	19
5.1.1	<i>Thin plate rectangular element (Non conforming).....</i>	<i>19</i>
5.1.2	<i>Heterosis elemet.....</i>	<i>20</i>
5.1.3	<i>Node to node connection.....</i>	<i>22</i>
5.1.4	<i>MPC connection.....</i>	<i>22</i>
5.2	Analytical solution.....	24
5.3	Numerical examples.....	25
5.3.1	<i>Influence of element size in MPC connections.....</i>	<i>29</i>
6	COMPONENT MODE SYNTHESIS APPLIED TO MPC CONNECTIONS....	31
6.1	Frequency response function.....	34
6.2	Numerical validation.....	35
7	CONCLUSIONS.....	40
8	AKNOWLEDGEMENTS.....	41
9	REFERENCES.....	41
	APPENDIX A.....	42
	APPENDIX B.....	44

1 INTRODUCTION

Structural elements such as beams, plates, rods, etc, are typically assembled together using elements called structural joints in order to build more complex structures. In the automotive industry one of the most important structural joints is the spot welded joint. A vehicle body contains several thousands of spot-welds. The properties and characteristics of these connecting elements contribute significantly to the overall dynamic behaviour of the structure, e.g. natural frequencies, mode shapes and frequency response functions (FRFs).

To perform the dynamic analysis of mechanical structures, the finite element (FE) method is typically used [1]. In order to include the participation of the joints it is necessary to use a model able to represent the dynamic characteristics of the spot welds. Modelling spot welds is a difficult task, mainly because there are many local effects such as geometrical irregularities, residual stresses, material inhomogeneities and defects due to the welding process that very difficult to take into account. Furthermore it is necessary to use models with as few DOFs as possible, since real spot welded structures usually possess many spot welds and modelling each of them in detail would lead to a major computational effort.

Commonly in FE models, point connections such as welds, rivets and bolts, are represented by two-noded elements (e.g. beams or springs with lumped masses). The parameters of these simple elements represent the mass and stiffness characteristics of the real joint, and therefore their influence on the rest of the structure. This simple connection can be connected to the substructures mainly in two different ways: (1) directly connect the joint nodes to nodes in the substructures (node-to-node connection) and (2) using interpolation elements or multipoint constraints (MPCs) to connect the joint nodes to the substructures. The node-to-node connection requires coincident meshes: if the location of the joint changes, then the mesh of both surfaces needs to be modified. In contrast, when interpolation elements or MPCs are used, the connection can be placed at any location using the existing surface meshes.

The latter feature offers a great advantage to industry, since it is then possible to assemble components with different mesh characteristics or to assemble components with complex geometries in which it is very difficult to have coincident nodes. Moreover, MPC connections can improve the computational efficiency when Monte Carlo simulation (MCS) is used to

analyze the dynamic behaviour of built-up structures with uncertainties in the location of the joints. In this case the MPC connections are used to model changes in the location of the joint instead of modifying the FE model from one sample to the next. In order to further improve the efficiency, component mode synthesis (CMS) gives a sub-structuring framework by which the number of the degrees of freedom (DOFs) can be reduced [2]. Combining CMS with MPC joints, the response of the system can be evaluated for many joint locations using the same modal representation of the substructures.

However, model validation is needed. In this document the results from FE models with MPCs are compared to analytical solutions to evaluate the accuracy of these modelled connections and to analyze the influence of the size and the type of element at which these MPCs are attached. Two different models are analyzed: two infinite beams and two simply supported plates. In all the models there is a single elastic connection with translational and rotational stiffnesses.

Following this introduction, a review of the different FE joint models available in the literature is given. In section 3 the MPC joint model is described in detail. In Section 4 the MPC joint model is validated using a model of two infinite beams with a single elastic connection. In Section 5 the MPC joint model is validated using a model of two simply supported plates with a single elastic connection and the influence of the size and the type of element at which these MPCs are attached is analyzed. Section 6 describes a method to apply component mode synthesis in combination with MPC joints to reduce the size of the model. Finally, conclusions are given in section 7.

2 SPOT WELD FINITE ELEMENT MODELS

A good FE spot weld model should be able to represent the physical and dynamic properties of these joints and therefore the variations in them. In this section some of the joint models available in the literature are reviewed.

Two main types of spot weld models can be distinguished: models for stress analysis within the spot weld and models for vibration analysis which do not require the knowledge of stresses at the spot welds. In the first case, very detailed models are required to compute a smooth stress field at the spot weld. As stated previously, these models are used for stress analysis and durability. In general they are too detailed to use in dynamic analysis, leading to a prohibitive computational cost, therefore these models will not be considered in the present document. In the second case the only requirement from the model is to simulate, as closely as possible, the stiffness (and mass) characteristics of the real spot welds and their influence on the rest of the structure. This allows much simpler models with far fewer DOFs.

These simpler models can be divided in two types, models that require coincident meshed surfaces in which the nodes of the plate elements of the joined surfaces are coincident and models that can be assembled with non-coincident meshes for which the plate nodes are non coincident, then it is not necessary to re-mesh surfaces to assemble them together.

Next some of the most common models are reviewed.

2.1 Single beam models

These models have been commonly used in industry for many years. A node to node connection is applied between coincident meshes using a rigid link or a beam element. According to Lardeur *et al.* [3] this connection is physically inconsistent and leads to imprecise and unstable results. Similarly Palmonella *et al.* [4] agree that this model is an inadequate representation for the behaviour of the spot weld and generally tends to underestimate its stiffness.

2.2 Single Brick model

This model was first proposed by Pal and Cronin [5] and connect two surfaces using a single brick element to characterise the spot weld nugget. The brick nodes are coincident with the plate nodes connected with rigid links in all DOFs, therefore it is necessary to have coincident meshes for the surfaces to be connected.

2.3 Area Contact Model 2

This element was created by Heiserer [6] and is known as area contact model 2 (ACM2). This model consists of a brick element connecting the lower and upper plates with weighted average constraint elements, called RBE3 in MSC Nastran [7], as shown in Figure 1. RBE3 defines the motion at a reference grid point as the weighted average of the motions at a set of other grid points. The RBE3 element is able to distribute the applied loads onto a set of nodes without increasing the local stiffness as would happen with a rigid link. The ACM2 model is also known as the CHEXA spot weld model in LMS virtual lab [8]. This model provides the advantage of being able to connect surfaces with non congruent meshes and locate the spot weld anywhere in the surface between nodes, but is relatively sensitive to mesh size [3].

2.4 CWELD

Fang *et al.* [9] proposed a model designed to connect congruent as well as non-congruent meshes using MPC equation. This element was implemented as the CWELD element in MSC/NASTRAN or PLINK in ESI/Pam-Crash. Figure 2 shows a sketch of the CWELD element. The elastic part of the CWELD element is a short beam from points GA to GB with six DOFs per node; this beam is modelled as a shear flexible Timoshenko type. The location of the connection is defined with a single grid point GS, which is projected onto the surfaces to be joined. Every node of the beam is connected to a chosen set of nodes of the plate to which it belongs. In Figure 2, the node GA for example is connected to the shell nodes GA1, GA2, GA3 and GA4 belonging to the upper plate. The portions of the plates delimited by the nodes GA_i and GB_i are called “patches” [7].

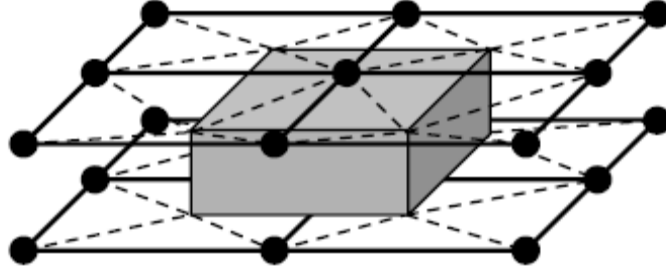


Figure 1: ACM2 model [3]

The DOFs of the spot weld end point GA are constrained as follows: the 3 translational and 3 rotational DOFs are connected to the 3 translational DOFs of each node GA_i with constraints from Kirchoff shell theory,

$$\begin{Bmatrix} u \\ v \\ w \end{Bmatrix}_A = \sum N_i(\xi_A, \eta_A) \cdot \begin{Bmatrix} u \\ v \\ w \end{Bmatrix}_i \quad (2.1)$$

$$\theta_x^A = \frac{\partial w}{\partial y} = \sum N_{i,y} \cdot w_i \quad (2.2)$$

$$\theta_y^A = \frac{\partial w}{\partial x} = -\sum N_{i,x} \cdot w_i \quad (2.3)$$

$$\theta_z^A = \frac{1}{2} \left(\frac{\partial v}{\partial x} - \frac{\partial u}{\partial y} \right) = \frac{1}{2} \left(\sum N_{i,x} \cdot v_i - \sum N_{i,y} \cdot u_i \right) \quad (2.4)$$

Here x, y and z are the co-ordinates, with z being perpendicular to the element plane; $N_{i,i}$ are the parametric shape functions; ξ_A and η_A are the normalised coordinates; $u, v,$ and w are the displacement DOFs and θ_x, θ_y and θ_z are rotational DOFs.

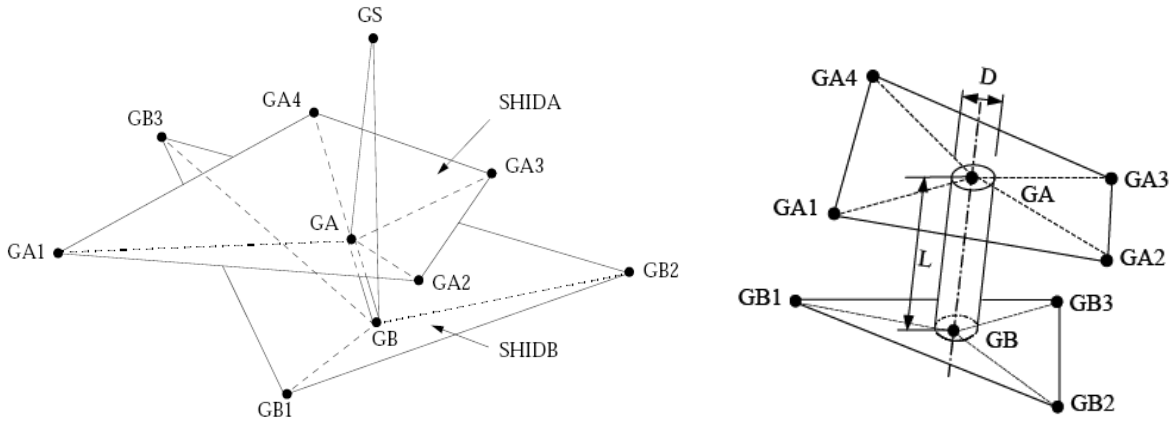


Figure 2: CWELD model [7]

2.5 Summary

Some of the most commonly used FE spot weld models were reviewed in this section. Their advantages and disadvantages are discussed next.

The CWELD and ACM2 models can be located anywhere in the model, while the beam and brick models can only be connected between existing nodes and require coincident meshed surfaces. It is clear that a connection that can be located anywhere in the model is preferable.

In the ACM2 and brick models, the joining element creates a link between areas in the connected plates. These areas can be related to the spot weld dimensions but controlled by the element size. In contrast the beam model creates a link between points. The CWELD model also creates a link between points, but the areas of the elements at which it is attached are constrained. It has been shown that a connection between points is not satisfactory when modelling spot welds, therefore a model that links areas is preferred.

The ACM2 model is connected using RBE3 elements, which define the displacement at a given location as the weighted average of the displacement at a set of other grid points. In contrast, the CWELD model uses an MPC which specifies a consistent displacement with the element formulation, this being preferred to the RBE3.

In general, the characteristics of the CWELD are appealing in contrast to other spot weld models and recently it has been used extensively. Finally a model based on MPC connections based on the CWELD model will be described and analyzed in the following sections.

3 MPC ELASTIC CONNECTION

An MPC elastic connection consists of spring elements connected to the substructures using MPCs. The MPCs relate the connection DOFs Δ' to the substructures' DOFs Δ involved in the joint (see Figure 3) using a set of equations, i.e.

$$\Delta' = \mathbf{G}(x', y')\Delta \quad (3.1)$$

where \mathbf{G} is the matrix of coefficients of the MPC equations, in this case \mathbf{G} is populated using the element shape functions. In doing so, the relationship between Δ' and Δ is made consistent with the FE formulation and is a function of the position of the joint within the element (x', y') .

There are many methods available in the literature to apply MPCs to the FE model, e.g. static condensation [10], augmented Lagrange multipliers, Lagrange elimination etc. When static condensation is used, a transformation matrix $\mathbf{\Gamma}$ that relates all the DOFs involved in the joint element can be written as,

$$\begin{Bmatrix} \Delta \\ \Delta' \end{Bmatrix} = \mathbf{\Gamma}\Delta \quad (3.2)$$

where

$$\mathbf{\Gamma} = \begin{bmatrix} \mathbf{I} \\ \mathbf{G} \end{bmatrix} \quad (3.3)$$

The DOFs Δ' are condensed into the DOFs Δ , resulting in a stiffness matrix

$$\mathbf{K}_{MPC} = \mathbf{\Gamma}^T \begin{bmatrix} \mathbf{K} & 0 \\ 0 & \mathbf{K}' \end{bmatrix} \mathbf{\Gamma} \quad (3.4)$$

where \mathbf{K}' is the connection stiffness matrix in local DOFs and \mathbf{K} is the stiffness matrix of the substructure DOFs involved in the connection, as can be observed in Figure 3.

The resulting nodal forces in the joint are

$$\mathbf{F} = \mathbf{K}_{MPC} \Delta \quad (3.5)$$

The substructures DOFs Δ can be partitioned as

$$\begin{bmatrix} \mathbf{F}_1 \\ \mathbf{F}_2 \end{bmatrix} = \begin{bmatrix} \mathbf{K}_{MPC}^{(11)} & \mathbf{K}_{MPC}^{(12)} \\ \mathbf{K}_{MPC}^{(21)} & \mathbf{K}_{MPC}^{(22)} \end{bmatrix} \begin{bmatrix} \Delta^{(1)} \\ \Delta^{(2)} \end{bmatrix} \quad (3.6)$$

where $\Delta^{(1)}$ and $\Delta^{(2)}$ are the DOFs in substructure (1) and substructure (2) respectively.

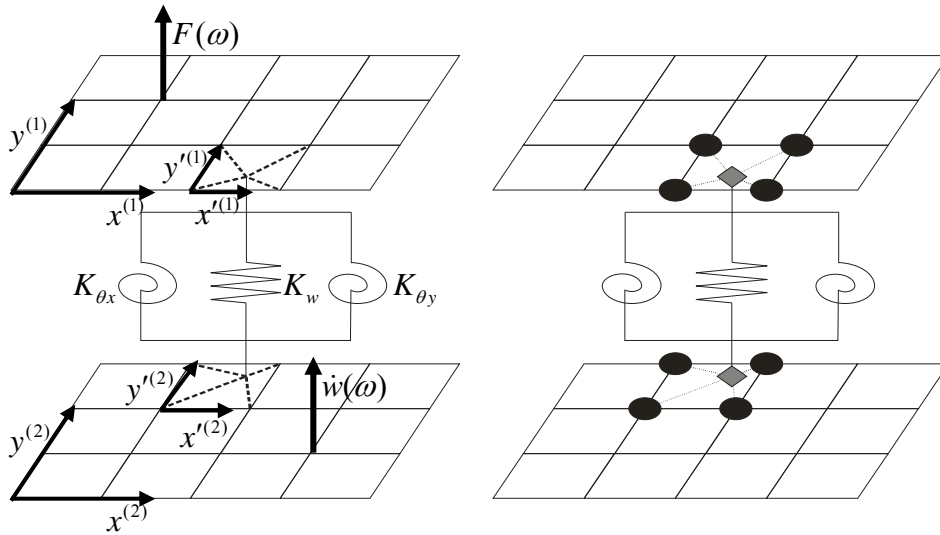


Figure 3: MPC elastic connection for plate bending analysis:
 ◆ joint DOFs (Δ'); ● substructure DOFs involved in the connection (Δ).

4 VALIDATION OF A MULTIPOINT CONSTRAINT SPOT-WELD MODEL FOR ONE DIMENSIONAL SYSTEMS.

This section investigates the validation of use of MPCs for connecting FE models and their ability to locate a connection anywhere between nodes. To avoid effects due to resonances and to simplify the evaluation, the joint is placed in a model of two infinite Euler-Bernoulli beams joined by a single connection. The transfer mobility from the upper to the lower beam as shown in Figure 4, is evaluated using two different FE models; one with an MPC elastic connection and the second with a node-to-node connection. Finally, the results are compared to an analytical solution.

4.1 Finite Element models

To model an infinite beam model, the region of the elastic connection is modelled using Euler-Bernoulli beam finite elements and then attached to semi-infinite Spectral Elements (SEs) as shown in Figure 5.

An infinite beam structure can be incorporated into the FE model using the SE method. The SE approach is similar to the FE method, but the element matrix is defined via the dynamic stiffness relationships in the frequency domain [11]. An SE element that extends to infinity and is connected at a single point can be created; this element simulates a semi-infinite medium and can be connected to any node in a FE model according to the method described by Doyle [11].

The dynamic stiffness matrix of a semi infinite beam that extends to $+\infty$ is given by

$$\mathbf{D}_{se}^1 = EI \begin{bmatrix} -(1-i)k_b^3 & ik_b^2 \\ ik_b^2 & (1+i)k_b \end{bmatrix} \quad x \geq 0 \quad (4.1)$$

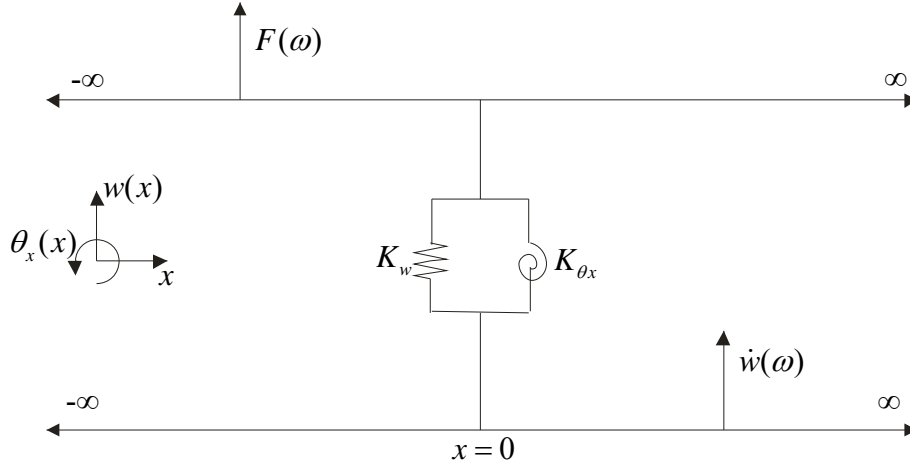


Figure 4: Two infinite beams connected with an elastic connection

where

$$k_b = \sqrt[4]{\frac{\omega^2 \rho A}{EI}} \quad (4.2)$$

is the beam wave number. In the same way the dynamic stiffness matrix for a beam that extends to $-\infty$ is given by

$$\mathbf{D}_{se}^2 = EI \begin{bmatrix} -(1-i)k_b^3 & -ik_b^2 \\ -ik_b^2 & (1+i)k_b \end{bmatrix} \quad x \leq 0 \quad (4.3)$$

The SEs are connected to the FEs in a similar way in which two FEs are connected, but instead of connecting the mass and stiffness matrices, the dynamic stiffness matrices of the FEs

$$\mathbf{D}_{fe} = \mathbf{K} - \omega^2 \mathbf{M} \quad (4.4)$$

are connected to the dynamic stiffness matrix of the SEs.

4.1.1 Node to node connection

The nodal force matrix \mathbf{F}' of a connecting element comprising a translational and a rotational spring can be expressed as

$$\mathbf{F}' = \mathbf{K}'\Delta' = \begin{bmatrix} K_w & 0 & -K_w & 0 \\ 0 & K_{\theta x} & 0 & -K_{\theta x} \\ -K_w & 0 & K_w & 0 \\ 0 & -K_{\theta x} & 0 & K_{\theta x} \end{bmatrix} \begin{Bmatrix} w_1' \\ \theta_{x1}' \\ w_2' \\ \theta_{x2}' \end{Bmatrix} \quad (4.5)$$

where \mathbf{K}' is the joint stiffness matrix in the local DOFs Δ' , K_w and $K_{\theta x}$ are the rotational and translational stiffness of the elastic connection as shown in Figure 5 and w_j and θ_{xj} are the local DOFs at node j . \mathbf{K}' can be transformed into global DOFs as

$$\mathbf{K}_{joint} = \mathbf{A}^T \mathbf{K}' \mathbf{A} \quad (4.6)$$

where \mathbf{K}_{joint} is the joint stiffness matrix in global co-ordinates and \mathbf{A} is a transformation matrix that relates the local to the global DOFs [1].

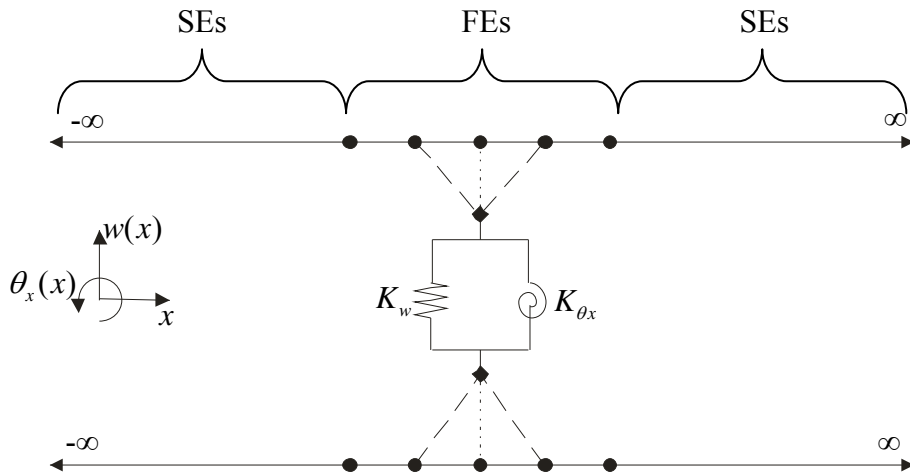


Figure 5: FE-SE Model of two infinite beams joined by a translational and a rotational spring

4.1.2 MPC connection

The local DOFs of the joint element in equation (4.5) can be related to one or more DOFs in the global matrices using a MPC equation. The same method described in section 3 can be used. In this case the model is assembled as shown in Figure 5 and the \mathbf{G} matrix in equation (3.3) is expressed as

$$\mathbf{G} = \begin{bmatrix} N_1(\xi^{(1)}) & aN_2(\xi^{(1)}) & N_3(\xi^{(1)}) & aN_4(\xi^{(1)}) & 0 & 0 & 0 & 0 \\ \frac{N_1'(\xi^{(1)})}{a} & N_2'(\xi^{(1)}) & \frac{N_3'(\xi^{(1)})}{a} & N_4'(\xi^{(1)}) & 0 & 0 & 0 & 0 \\ 0 & 0 & 0 & 0 & N_1(\xi^{(2)}) & aN_2(\xi^{(2)}) & N_3(\xi^{(2)}) & aN_4(\xi^{(2)}) \\ 0 & 0 & 0 & 0 & \frac{N_1'(\xi^{(2)})}{a} & N_2'(\xi^{(2)}) & \frac{N_3'(\xi^{(2)})}{a} & N_4'(\xi^{(2)}) \end{bmatrix} \quad (4.7)$$

where

$$N_1(\xi) = \frac{1}{4}(2 - 3\xi + \xi^3) \quad (4.8)$$

$$N_2(\xi) = \frac{1}{4}(1 - \xi - \xi^2 + \xi^3) \quad (4.9)$$

$$N_3(\xi) = \frac{1}{4}(2 + 3\xi - \xi^3) \quad (4.10)$$

$$N_4(\xi) = \frac{1}{4}(-1 - \xi + \xi^2 + \xi^3) \quad (4.11)$$

are the parametric shape functions for a FE Euler-Bernoulli beam and

$$\xi^{(i)} = \left(\frac{x^{(i)} - a}{a} \right) \quad (4.12)$$

is the normalized co-ordinate for beam i , $a = s/2$ where s is the element length.

4.2 Analytical solution

Appendix A gives the equations governing the system in Figure 4 using a mobility approach, and it also describes the derivation of the transfer mobility from a force excitation applied at point 1 on the first beam to a response evaluated at point 4 on the second beam.

Solving the equations in appendix B, the velocities of beams 1 and 2 at the connection point are given by

$$\begin{bmatrix} \mathbf{V}_C^{(1)} \\ \mathbf{V}_C^{(2)} \end{bmatrix} = \left[\mathbf{I} - \begin{bmatrix} \mathbf{Y}_{2,2}^{(1)} & 0 \\ 0 & \mathbf{Y}_{3,4}^{(2)} \end{bmatrix} \mathbf{Z}_c \right]^{-1} \begin{bmatrix} \mathbf{Y}_{1,2}^{(2)} \\ 0 \end{bmatrix} \mathbf{F}_{ext} \quad (4.13)$$

where

$$\mathbf{Z}_c = i\omega \begin{bmatrix} K_w & 0 & -K_w & 0 \\ 0 & K_{\theta x} & 0 & -K_{\theta x} \\ -K_w & 0 & K_w & 0 \\ 0 & -K_{\theta x} & 0 & K_{\theta x} \end{bmatrix} \quad (4.14)$$

is the impedance of the connection and

$$\mathbf{Y}_{i,j}^{(k)} = \begin{bmatrix} Y_{i,j}^{v,F} & Y_{i,j}^{v,M} \\ Y_{i,j}^{\psi,F} & Y_{i,j}^{\psi,M} \end{bmatrix} \quad (4.15)$$

is the mobility matrix from point i to point j for the k^{th} Euler-Bernoulli beam.

4.3 Numerical examples

The numerical example is a system of two infinite beams joined together by an elastic connection. To simplify the analysis all simulations were divided into two cases, the first in which only the effects of a translational spring K_w are analyzed and the second in which only

K_{θ_x} is considered in order to analyze the effects of a rotational spring. The values used for K_w and K_{θ_x} are 10^6 N/m and 10^4 Nm/rad respectively. Both beams were assumed to be identical and the properties are given in Table 1.

When the mobility of the translational connection is compared to the imaginary part of the mobility of the connected beams, a critical frequency ω_0 can be found, i.e.

$$\omega_0 = \left(\frac{K_T}{2EI} \right)^{\frac{2}{3}} \left(\frac{EI}{\rho A} \right)^{\frac{1}{2}} \quad (4.16)$$

below ω_0 the spring is effectively rigid and the behaviour of the assembly is that of two beams working in parallel, above ω_0 the spring is flexible and works as an isolator.

When the mobility of the rotational connection is compared to the imaginary part of the mobility of the connected beams, two critical frequencies appear ω_1 and ω_2 , i.e.

$$\omega_1 = \frac{K_R^2}{2(\rho A)^{1/2} (EI)^{3/2}} \text{ and } \omega_2 = \left(\frac{1}{x_e + x_r} \right)^2 \cdot \left(\frac{EI}{\rho A} \right)^{\frac{1}{2}} \quad (4.17)$$

Given the stiffness value and the beams properties used in the present example, $\omega_0 = 654$ rad/s, $\omega_1 = 81.56$ rad/s and $\omega_2 = 11574$ rad/s.

The transfer mobility from the upper beam a position $x = -0.01$ m in the upper beam to a position $x = 0.01$ m in the lower beam was evaluated using two different FE models; the first using a MPC connection and the second using a node to node connection. Finally both solutions were compared to the analytical result.

	Cross Section	b (m)	h (m)	ρ (Kg/m ³)	E (N/m ²)	ν
Beams (1&2)	Rectangular	0.5	0.006	7860	2.07E+11	0.3

Table 1: Beam properties

4.3.1 Accuracy of FE models: a single translational spring connection.

Figure 6 shows the comparison between the results from both FE models and the analytical solution for the translational stiffness case. When the spring is connected from node to node (see Figure 5), the result for the transfer mobility is not exact due to FE discretization errors.

In Figure 6, the mobility is plotted using a non dimensional frequency $(k_b s)^2$ for the abscissa. In doing so, it is possible to compare the accuracy of different FE models with different element size; the frequencies corresponding to $s=\lambda/6$, $s=\lambda/3$ and $s=\lambda$ are added as reference. Figure 6 shows the comparison between the exact solution and the prediction using the FE-SE model. It can be seen that the prediction agrees with the exact solution and it starts to deviate for frequencies slightly above the frequencies where $s > \lambda/3$. If $s > \lambda$ the solution is very inaccurate. These errors are expected from any FE model, since as a rule of thumb the predictions from a FE model are accurate up to a frequency for which $s=\lambda/6$. If the element shape functions are quadratic, as used in this study, then the accuracy limit increases up to frequencies where $s = \lambda/3$.

When the results from the MPC connection model are compared, it can be seen that the prediction agrees very well with the exact solution and start to differ at frequencies slightly lower than frequencies where $s > \lambda/3$; therefore it is marginally less accurate than the node to node connection. This is explained by the fact that the displacements of the connection nodes depend on the shape functions of the element to which it is connected when a MPC is used; therefore additional discretization errors are introduced into the solution.

However, these additional errors are small and the agreement between both models is very good at low frequencies, especially at frequencies corresponding to $s < \lambda/6$.

4.3.2 Accuracy of FE models: a single rotational spring connection

When the node to node connection is used, the transfer mobility can be predicted with good accuracy at low frequencies as can be seen in Figure 7. The solution obtained with the node to node FE-SE model is accurate for frequencies where $s < \lambda/3$. At higher frequencies, the

solution starts to deviate from the analytical solution. Similar to the translational stiffness connection, when a MPC connection is used to connect the rotational spring, the response starts to deviate significantly from the analytical solution at slightly lower frequencies compared to the node to node connection.

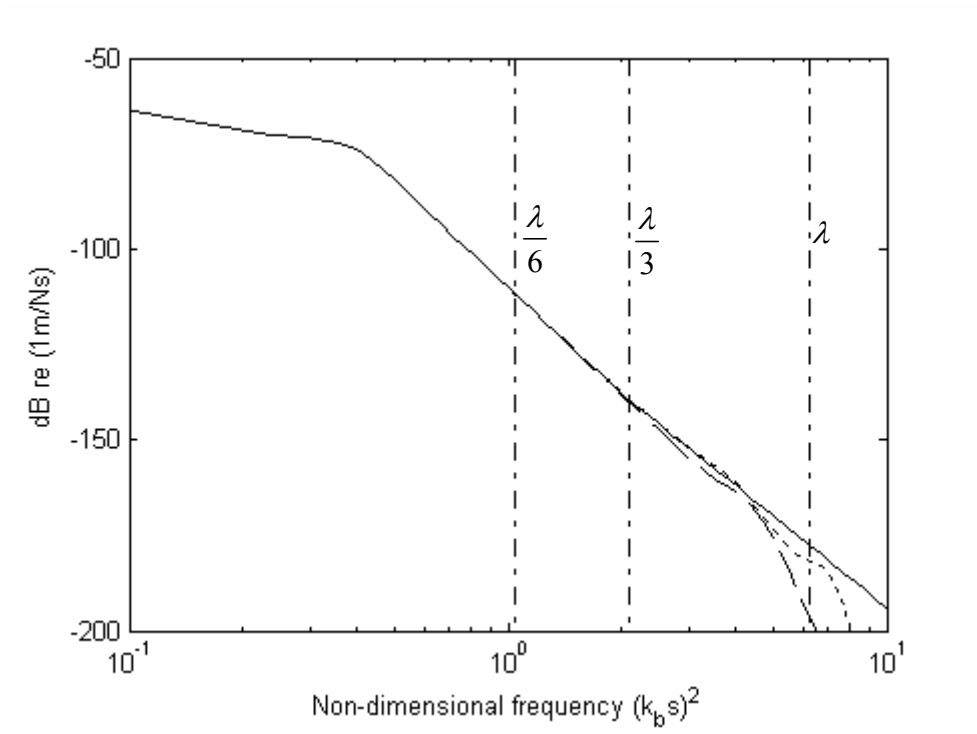


Figure 6: Transfer mobility magnitude in a system of two infinite beams with a single elastic translational connection: — analytical solution; --- MPC connection; ----- node to node connection.

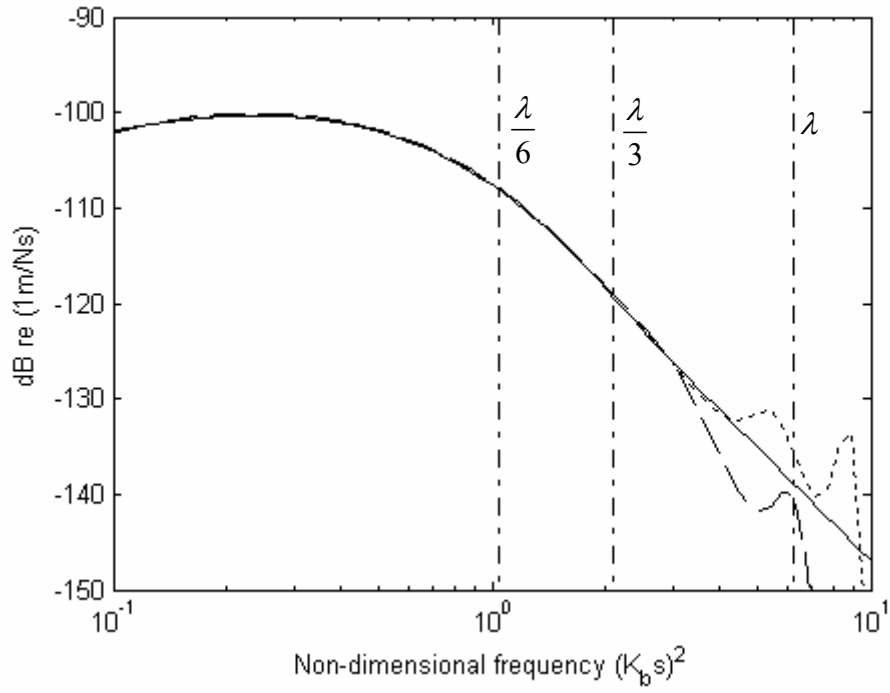


Figure 7: Transfer mobility magnitude in a system of two infinite beams with a single elastic rotational connection: — analytical solution; --- MPC connection; node to node connection.

5 VALIDATION OF A MULTIPOINT CONSTRAINT SPOT-WELD MODEL FOR TWO DIMENSIONAL SYSTEMS.

When plates are connected with an MPC joint, the MPC coefficient matrices are populated with the element shape functions as can be observed in equations (2.1) to (2.4) and in section 3. Therefore it is important to analyze the formulation of the plate element that is being used.

There are two main different plate theories [12]. The first is Kirchoff plate theory, in which the effects of transverse shear deformation and rotary inertia are neglected. Kirchoff plate theory is applicable to thin plates in which the plate thickness is much smaller than the bending wavelength. The second is Mindlin-Reissner theory. Here the transverse shear and rotary inertia become important when describing the plate behaviour, and is often used to analyze thick plates.

When Kirchoff plate theory is used, the element results in a non-conforming formulation or alternately in a conforming formulation with additional DOFs [1]; the non-conforming formulation could result in incompatibilities with the MPC equations, whilst the conforming formulation is difficult to assemble due to the additional DOFs.

Alternatively, when Mindlin-Reissner theory is used [12], the transverse shear strain is independent of the thickness of the plate. Therefore as the plate thickness decreases, the strain energy associated with transverse shear tends to dominate the response, rather than tending to zero as in the Kirchoff plate theory. This phenomenon is referred to as “shear locking” and leads to an overly stiff prediction of the response. One approach to reducing the effects of shear locking is to use a reduced number of Gauss integration points when evaluating the shear stiffness of an element [13, 14]. In effect, this reduces the order of the interpolation for the transverse shear strain to that used in the Gauss integration scheme. In general this approach can lead to rank deficiency of the stiffness matrix and a singular set of equations. However, by appropriate selection of the element basis functions and integration schemes, it is possible to obtain a robust element known as the Heterosis plate element [15].

In this section the ability of the MPC connection to be located anywhere in an element is tested for two different element formulations, namely a non-conforming thin plate rectangular element [1] and a heterosis plate element [13].

A system of two simply supported plates with a single elastic connection is used. The transfer mobility from the upper plate to the lower plate is evaluated using two different FE models; one with an MPC elastic connection and the second with a node-to-node connection. Results are then compared to an analytical solution.

5.1 Finite element models

5.1.1 Thin plate rectangular element (Non conforming)

This is a four noded element, with one node at each corner. Each node has three DOFs which describe flexural motion, vertical displacement w and two rotations θ_x and θ_y as can be observed in Figure 8. It is based on Kirchoff plate theory, therefore it is assumed that

$$\theta_x = \frac{\partial w}{\partial y} \text{ and } \theta_y = -\frac{\partial w}{\partial x} \quad (5.1)$$

the displacement function can be described in terms of the normalised coordinates ξ and η as

$$w = [\mathbf{N}_1(\xi, \eta) \quad \mathbf{N}_2(\xi, \eta) \quad \mathbf{N}_3(\xi, \eta) \quad \mathbf{N}_4(\xi, \eta)] \mathbf{w}_e \quad (5.2)$$

where \mathbf{w}_e is a vector that contains the element DOFs and

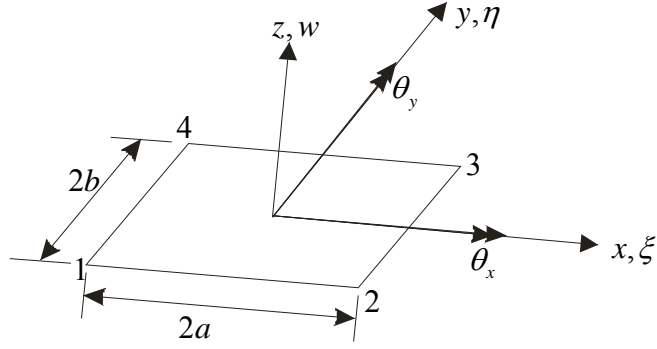


Figure 8: Geometry of a rectangular element

$$\mathbf{N}_j^T(\xi, \eta) = \begin{bmatrix} \frac{1}{8}(1 + \xi_j \xi)(1 + \eta_j \eta)(2 + \xi_j \xi + \eta_j \eta - \xi^2 - \eta^2) \\ \frac{b}{8}(1 + \xi_j \xi)(\eta_j + \eta)(\eta^2 - 1) \\ \frac{a}{8}(1 + \eta_j \eta)(\xi_j + \xi)(\xi^2 - 1) \end{bmatrix} \quad (5.3)$$

are the element shape functions, where (ξ_j, η_j) are the normalized coordinates of each one of the element nodes.

The rotations θ_x and θ_y are evaluated using equations (5.1) and (5.2), when doing so it is noted that θ_y is determined by the values of w and θ_x at the four nodes as well as by the values of θ_y at nodes 2 and 3. This indicates that when elements are assembled, θ_y is discontinuous between nodes; this is therefore a non-conforming element.

5.1.2 Heterosis element

The Heterosis plate element [13] is a nine-noded plate element that is based on Mindlin - Reissner plate theory shown in Figure 9. The central node has two rotations and each other node has 5 DOFs which describe in-plane and out-of-plane motion (42 DOF in total). The displacement field within the element is interpolated using serendipity basis functions, whilst the rotations in the x and y directions are interpolated using Lagrange basis functions. Reduced order integration is used to evaluate the shear stiffness matrix. This element does not suffer from shear locking and possesses correct rank.

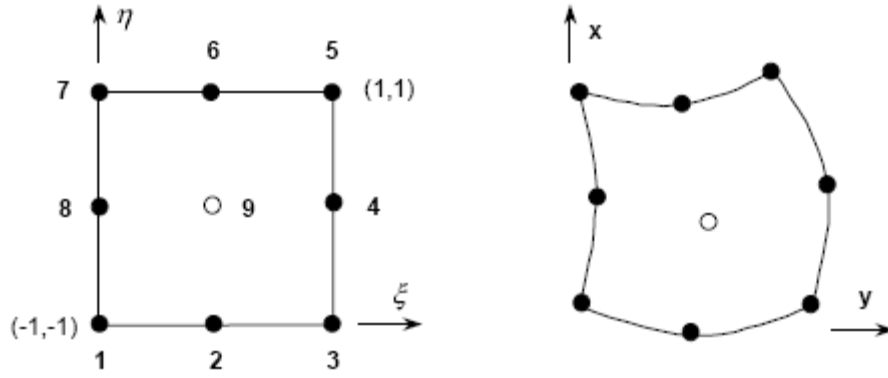


Figure 9: Node numbering for Heterosis element.

The out of plane co-ordinates (w, θ_x, θ_y) of a point within the element can be described as

$$w = \sum_{j=1}^8 N_j w_j \quad (5.4)$$

$$\theta_x = \sum_{j=1}^9 P_j \theta_{x,j} \quad (5.5)$$

$$\theta_y = \sum_{j=1}^9 P_j \theta_{y,j} \quad (5.6)$$

where j indicates the node number and

$$N_j = \frac{1}{4}(1 + \xi_j \xi)(1 + \eta_j \eta)(\xi_j \xi + \eta_j \eta - 1), \quad j = 1, 3, 5, 7 \quad (5.7)$$

$$N_j = \frac{\xi_j^2 (1 + \xi_j \xi)(1 - \eta^2)}{2} + \frac{\eta_j^2 (1 + \eta_j \eta)(1 - \xi^2)}{2}, \quad j = 2, 4, 6, 8 \quad (5.8)$$

$$P_j = \left(\frac{\xi_j \xi (1 + \xi_j \xi)}{2} + (1 - \xi^2)(1 - \xi_j^2) \right) \left(\frac{\eta_j \eta (1 + \eta_j \eta)}{2} + (1 - \eta^2)(1 - \eta_j^2) \right) \quad (5.9)$$

are vectors of Lagrange and Serendipity basis functions respectively.

5.1.3 Node to node connection

In the case of thin plate substructures with out-of-plane DOFs w , θ_x and θ_y , the elastic element contains a translational stiffness K_w and two rotational stiffnesses K_{θ_x} and K_{θ_y} , as shown in Figure 3.

The nodal forces and DOFs of the point connection are related by

$$\mathbf{F}' = \mathbf{K}'\mathbf{\Delta}' = \begin{bmatrix} K_w & 0 & 0 & -K_w & 0 & 0 \\ 0 & K_{\theta_x} & 0 & 0 & -K_{\theta_x} & 0 \\ 0 & 0 & K_{\theta_y} & 0 & 0 & -K_{\theta_y} \\ -K_w & 0 & 0 & K_w & 0 & 0 \\ 0 & -K_{\theta_x} & 0 & 0 & K_{\theta_x} & 0 \\ 0 & 0 & -K_{\theta_y} & 0 & 0 & K_{\theta_y} \end{bmatrix} \begin{Bmatrix} w_1' \\ \theta_{x1}' \\ \theta_{y1}' \\ w_2' \\ \theta_{x2}' \\ \theta_{y2}' \end{Bmatrix} \quad (5.10)$$

where \mathbf{K}' is the stiffness matrix of the point connection and $\mathbf{\Delta}'$ is a vector of local DOFs.

\mathbf{K}' can be transformed into global DOFs as

$$\mathbf{K}_{joint} = \mathbf{A}^T \mathbf{K}' \mathbf{A} \quad (5.11)$$

where \mathbf{K}_{joint} is the joint stiffness matrix in global co-ordinates and \mathbf{A} is a transformation matrix that relates the local to the global DOFs [1].

5.1.4 MPC connection

The local DOFs of the joint element in equation (5.10) can be related to one or more DOFs in the global matrices using a MPC equation. The method outlined in section 3 is used. In this case the model is assembled as shown in Figure 3, where the \mathbf{G} matrix in equation (3.3) is defined as

$$\mathbf{G} = \begin{bmatrix} \mathbf{G}^{(1)} & 0 \\ 0 & \mathbf{G}^{(2)} \end{bmatrix} \quad (5.12)$$

where $\mathbf{G}^{(i)}$ is the matrix that relates $\Delta^{(i)}$ to $\Lambda^{(i)}$ for substructure i . $\mathbf{G}^{(i)}$ depends on the element formulation

$$\mathbf{G}^{(i)}(x^{(i)}, y^{(i)}) = \begin{bmatrix} \mathbf{N}_1 & \mathbf{N}_2 & \mathbf{N}_3 & \mathbf{N}_4 \\ \frac{\partial \mathbf{N}_1}{\partial y} & \frac{\partial \mathbf{N}_2}{\partial y} & \frac{\partial \mathbf{N}_3}{\partial y} & \frac{\partial \mathbf{N}_4}{\partial y} \\ -\frac{\partial \mathbf{N}_1}{\partial x} & -\frac{\partial \mathbf{N}_2}{\partial x} & -\frac{\partial \mathbf{N}_3}{\partial x} & -\frac{\partial \mathbf{N}_4}{\partial x} \end{bmatrix} \quad (5.13)$$

where \mathbf{N}_j are the element shape functions for node j as defined in equation (5.3). When heterosis elements are used, $\mathbf{G}^{(i)}$ is defined as

$$\mathbf{G}^{(i)} = \begin{bmatrix} \mathbf{N}^{(i)} & 0 & 0 \\ 0 & \mathbf{P}^{(i)} & 0 \\ 0 & 0 & \mathbf{P}^{(i)} \end{bmatrix} \quad (5.14)$$

where

$$\mathbf{P}^{(i)} = [\mathbf{P}_1 \ \mathbf{P}_2 \ \mathbf{P}_3 \ \mathbf{P}_4 \ \mathbf{P}_5 \ \mathbf{P}_6 \ \mathbf{P}_7 \ \mathbf{P}_8 \ \mathbf{P}_9] \quad (5.15)$$

is the vector of serendipity basis functions for substructure as defined in equation (5.9) and

$$\mathbf{N}^{(i)} = [N_1 \ N_2 \ N_3 \ N_4 \ N_5 \ N_6 \ N_7 \ N_8] \quad (5.16)$$

is the vector of Lagrange basis functions for substructure i as defined in equations (5.7) and (5.8).

5.2 Analytical solution

In this section the transfer mobility for the system in Figure 10 is derived, thin plate theory being used.

Appendix B shows the equations governing the system in Figure 10 using a mobility approach, and it also describes the derivation of the transfer mobility from a force excitation applied at point 1 on the first plate to a response evaluated at point 4 on the second plate.

Solving equations in appendix A, the velocities at plate 1 and plate 2 at the connection are given by

$$\begin{bmatrix} \mathbf{V}_C^{(1)} \\ \mathbf{V}_C^{(2)} \end{bmatrix} = \left[\mathbf{I} - \begin{bmatrix} \mathbf{Y}_{2,2}^{(1)} & \mathbf{0} \\ \mathbf{0} & \mathbf{Y}_{3,4}^{(2)} \end{bmatrix} \mathbf{Z}' \right]^{-1} \begin{bmatrix} \mathbf{Y}_{1,2}^{(2)} \\ \mathbf{0} \end{bmatrix} \mathbf{F}_{ext} \quad (5.17)$$

where

$$\mathbf{Z}' = i\omega \mathbf{K}' \quad (5.18)$$

is the transfer impedance of the connection, and

$$\mathbf{Y}_{i,j}^{(k)} = \begin{bmatrix} Y_{i,j}^{w,F} & Y_{i,j}^{w,M_x} & Y_{i,j}^{w,M_y} \\ Y_{i,j}^{\theta_x,F} & Y_{i,j}^{\theta_x,M_x} & Y_{i,j}^{\theta_x,M_y} \\ Y_{i,j}^{\theta_y,F} & Y_{i,j}^{\theta_y,M_x} & Y_{i,j}^{\theta_y,M_y} \end{bmatrix} \quad (5.19)$$

are the mobility matrices from point i to point j for plate k . The terms in matrix (5.19) are calculated for thin rectangular plates in terms of a modal summation [16].

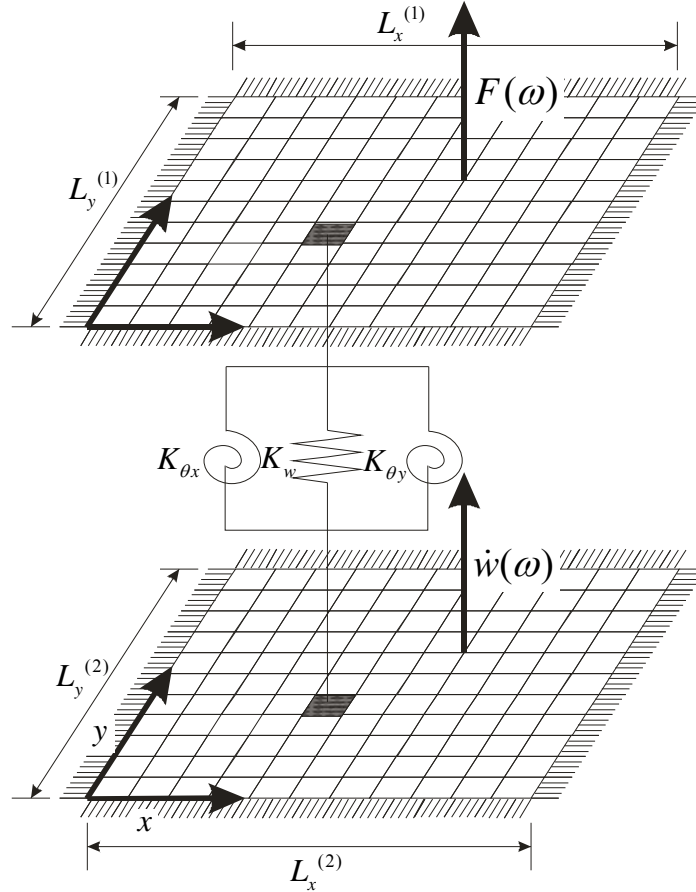


Figure 10: Two parallel simply supported plates assembled with an elastic point connection.

	L_x (m)	L_y (m)	h (m)	ρ (Kg/m ³)	E (N/m ²)	ν	η
Component (1)	0.6	0.5	0.006	7860	2.07E+11	0.3	0.02
Component (2)	0.6	0.5	0.02	7860	2.07E+11	0.35	0.02

Table 2: Properties of each component for the numerical example

5.3 Numerical examples

The numerical example is a system of two simply supported parallel plates with an elastic connection as shown in Figure 10. The properties for each plate are given in Table 2. To simplify the analysis all simulations were divided into two cases; the first in which only the effects of a translational spring K_w are analyzed and the second in which only K_{θ_x} is considered in order to analyze the effects of a rotational spring. The values used for K_w and K_{θ_x} are 16000 N/m and 1600 Nm/rad respectively.

The transfer mobility from coordinate (0.38, 0.32) in plate 1 to coordinate (0.38, 0.32) in plate 2 as shown in Figure 10 was evaluated. In this example, the co-ordinates of the spring (x_c, y_c) are (0.1227, 0.1614) in both plates.

When the MPC connection is incorporated, the plates are modelled using a mesh of 11×11 identical elements. The co-ordinates of the spring correspond to $(2.25 s_x, 3.5 s_y)$, where s_x is the element length in x direction and s_y is the element size in y direction. The local co-ordinates of the connection within the element are $(x', y') = (0.25 s_x, 0.5 s_y)$. For the node to node connection a mesh of 22×22 elements is used in order to have a node exactly at the elastic connection location.

When heterosis elements are used to predict the transfer mobility, in the case of a connection with translational stiffness K_w , both connection models have almost identical behaviour and are in very good agreement when compared to the analytical solution. Only FE discretization errors are present at higher frequencies as can be observed in Figure 11. At resonance the difference in magnitude is negligible and the first natural frequency is overestimated by approximately 0.5 Hz, whilst the second natural frequency is overestimated by approximately 0.3 Hz as shown in Figure 12(a) and Figure 12(b). These differences are small and consistent between FE models.

In the case of a connection with rotational stiffness K_{θ_x} , both connection models have good agreement with each other, but there are differences when compared to the analytical solution, especially at low frequencies where a difference of approximately 2dB can be observed in Figure 13. These discrepancies are mainly caused by the difference between the thin plate theory used in the analytical solution and the formulation of the heterosis element, which is based on Mindlin–Reissner theory, and convergence issues in the modal summation when rotational DOFs are involved. The natural frequencies are overestimated by the same amount as in the translational stiffness case, as can be observed in Figure 14.

In spite of these differences, the performance of the heterosis elements connected by MPCs is acceptable, having the same frequency limitation as typical FE models.

When thin plate elements are assembled using a node to node connection, the predictions are comparable to the results obtained from the heterosis element. In some cases this prediction is closer to the analytical solution, as can be observed in Figures 11 to 14 since both are based on thin plate theory. On the other hand, when thin plates are connected using MPCs the solution is significantly in error and different from the analytical solution, as can be observed in Figure 11 and Figure 12. The error is generated when the MPCs are attached to the non-conforming elements, for which θ_y is discontinuous between nodes. Hence an important overall conclusion is that MPC connections should not be implemented on any model comprising thin plate non-conforming elements.

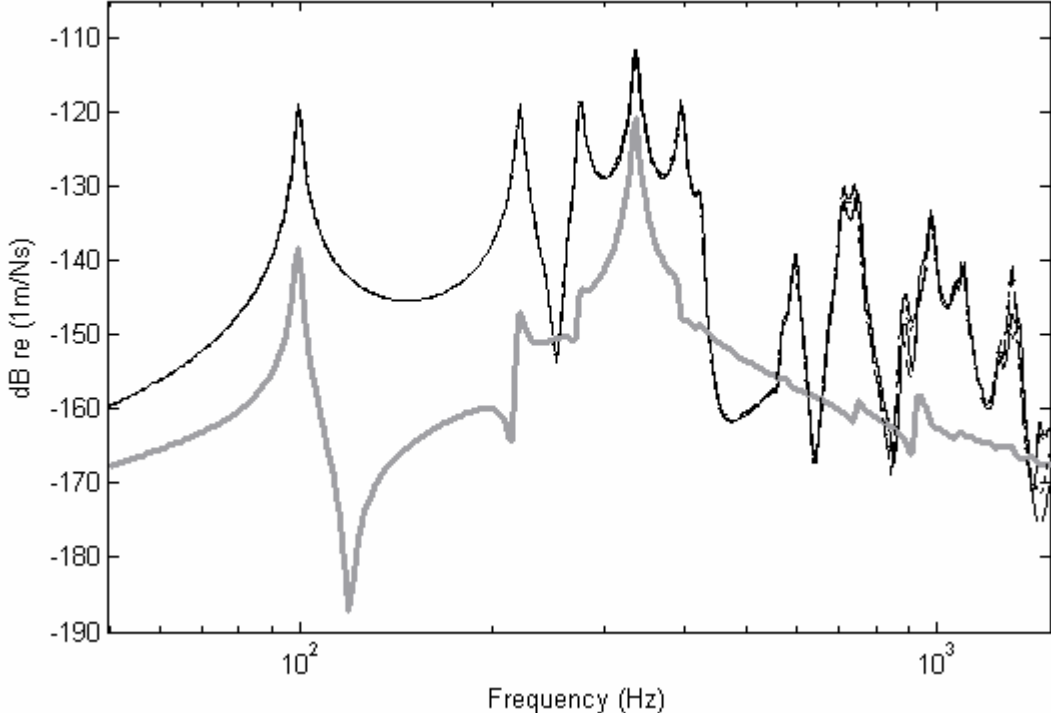


Figure 11: Magnitude of transfer mobility in a system of two simply supported plates with a single elastic connection with translational stiffness: — analytical solution; - - - node to node-heterosis; - · - · MPC-heterosis; · · · · node to node-thin; — MPC-thin.

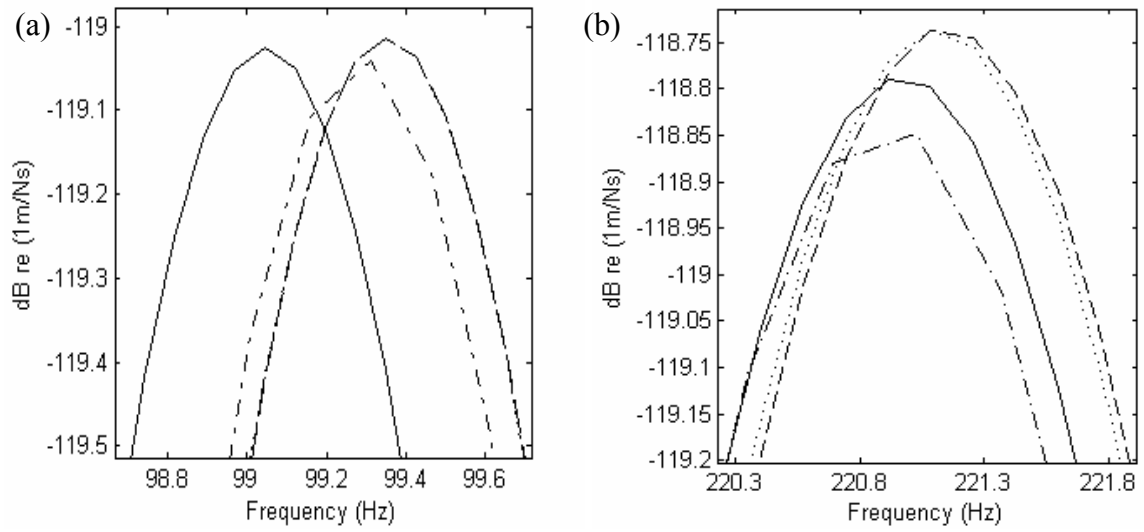


Figure 12: Magnitude of transfer mobility in a system of two simply supported plates with a single elastic connection with translational stiffness: (a) first resonance ; (b) second resonance: — analytical solution; node to node-heterosis; --- MPC-heterosis; -.-.- node to node-thin; — MPC-thin.

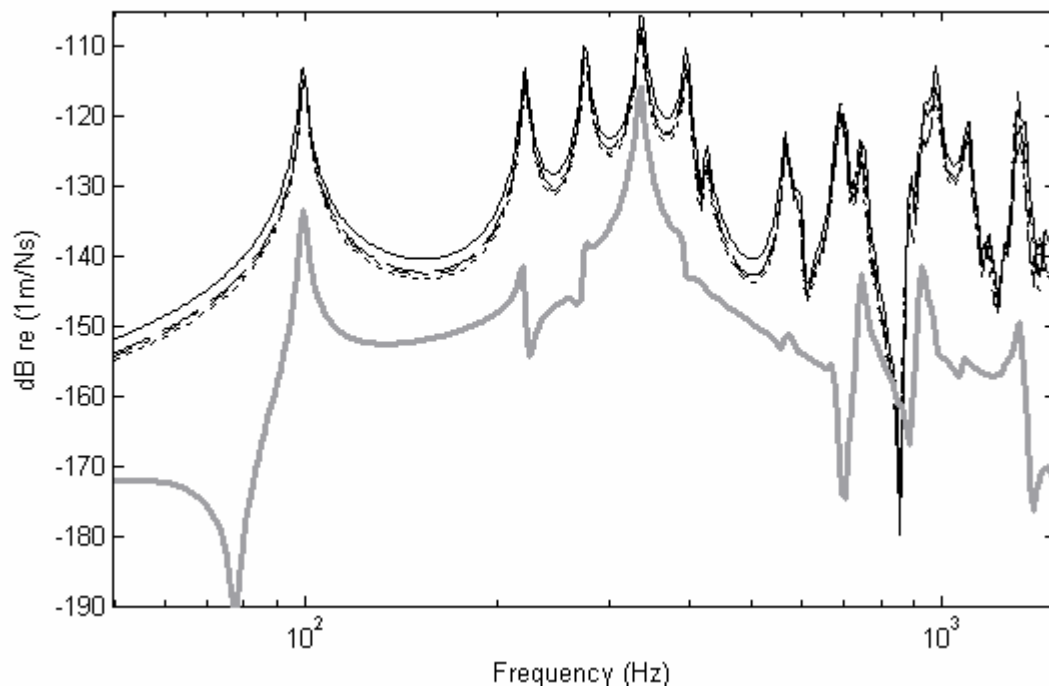


Figure 13: Magnitude of transfer mobility in a system of two simply supported plates with a single elastic connection with rotational stiffness: — analytical solution; node to node-heterosis; --- MPC-heterosis; -.-.- node to node-thin; — MPC-thin.

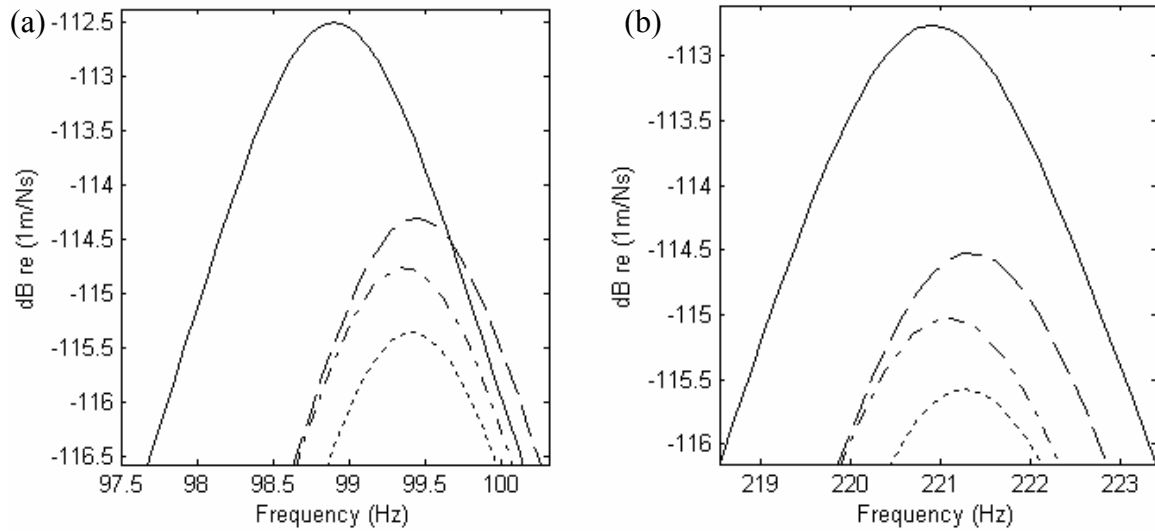


Figure 14: Magnitude of transfer mobility in a system of two simply supported plates with a single elastic connection with rotational stiffness: (a) first resonance; (b) second resonance:
— analytical solution;
..... node to node-heterosis; --- MPC-heterosis; - · - · - node to node-thin; — MPC-thin.

5.3.1 Influence of element size in MPC connections

To study the influence of element size for MPC connections, the same numerical example in section 5.4 was used. The FE model with heterosis elements and an MPC connection was modified to change the element size from the original 11×11 element mesh to meshes ranging from 6×6 to 22×22 elements and compared to the analytical solution.

Since the location of the nodes is changed for every different mesh, the force was applied and the response calculated using MPCs in order to predict the same transfer mobility as in section 5.4.

It was found that the element size has a small influence when adapting MPC connections and only differences at higher frequencies are present due to discretization errors as can be observed in Figure 15. There is a stiffening effect due to the increase in the constraint area as the element gets larger; however this effect is negligible since the variations in natural frequency and peak magnitude are insignificant as can be observed in Figure 16. It was also observed that MPCs not only can be used to locate and incorporate connections, but also to apply excitation forces and calculate responses at any location, leading to accurate transfer mobility calculations.

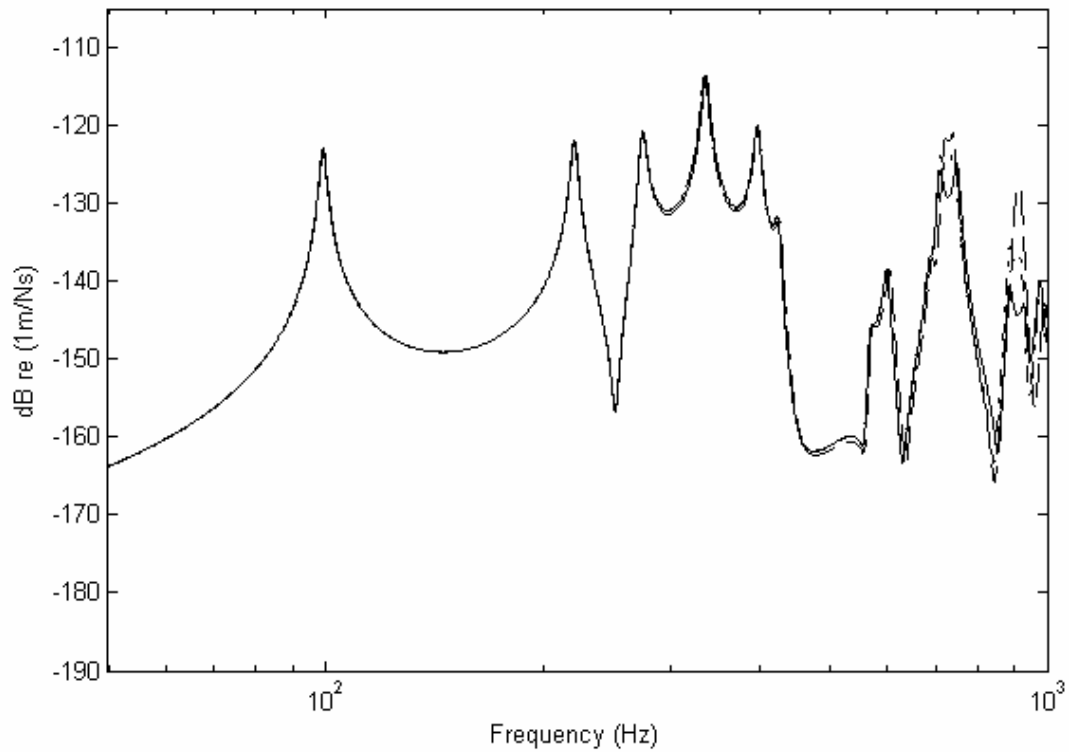


Figure 15: Transfer mobility magnitude in a system of two simply supported plates with a single elastic connection with translational stiffness: — analytical solution; - - - MPC-heterosis 6×6 mesh; - - - MPC-heterosis 22×22 mesh.

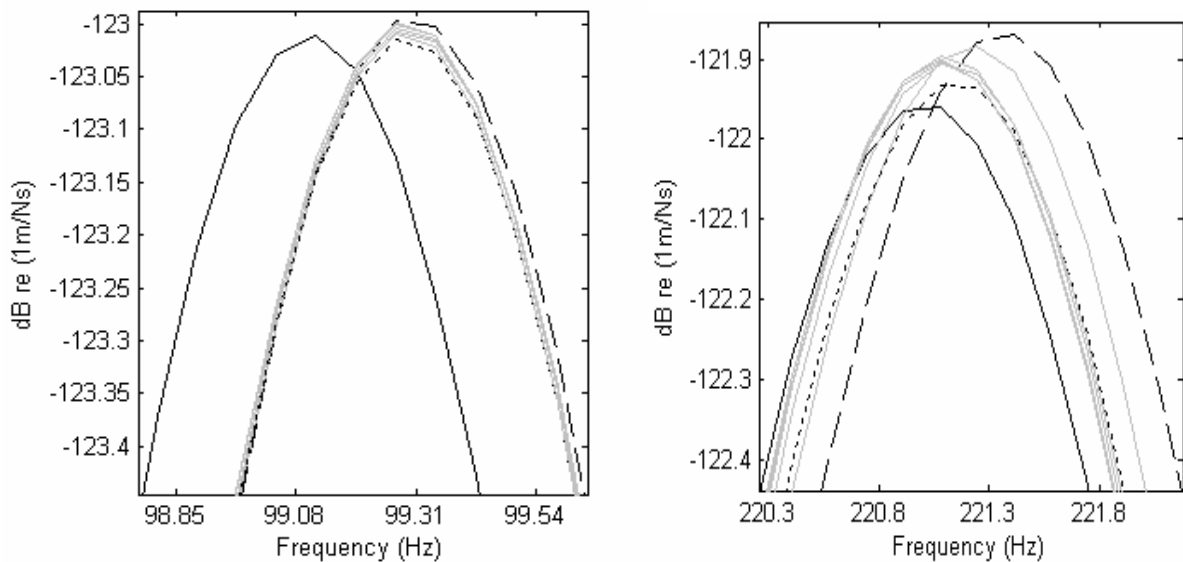


Figure 16: Transfer mobility magnitude in a system of two simply supported plates with a single elastic connection with translational stiffness: (a) first resonance; (b) second resonance: — analytical solution; - - - MPC-heterosis 6×6 mesh; - - - MPC-heterosis 22×22 mesh; — MPC-heterosis meshes from 7×7 to 21×21

6 COMPONENT MODE SYNTHESIS APPLIED TO MPC CONNECTIONS

CMS is a method used to reduce the size of the model and it also offers a sub-structuring framework for the analysis of the dynamic behaviour of uncertain structures [2]. One of the most accurate and frequently used CMS methods is the Craig-Bampton method [17]. In the fixed interface method the component normal modes are calculated with the interface between the components held fixed. These modes are further augmented by static constraint modes to improve convergence, yield the exact static solution and assure the compatibility between components, facilitating coupling of structures.

To use CMS with sub-structures assembled with an MPC connection, first the system is divided into components. For the example in Figure 10, the system can be divided into two components: (1) the upper plate and (2) the lower plate.

The second step is to constrain the interface DOFs in each component. Here all the DOFs surrounding the area in which the location of the connection varies are constrained. For example, Figure 17 shows the interface DOFs in the case in which the location varies within one element. The normal modes are then calculated and the reduced normal mode matrix for kept modes Φ_k^α is used. Here the reduction in size is achieved. The static constraint modes Ψ_c^α are evaluated and assembled in the overall component mode matrix

$$\mathbf{B}^i = \begin{bmatrix} \Phi_k^i & \Psi_c^i \end{bmatrix} \quad (6.1)$$

for component i , $i=1,2$. Then to transform from the component physical co-ordinates \mathbf{u} to the component modal co-ordinates \mathbf{q} then

$$\mathbf{u} = \mathbf{B}\mathbf{q} \quad (6.2)$$

The component modal mass and stiffness matrices for each component i are given by,

$$\boldsymbol{\mu}^i = \mathbf{B}^{iT} \mathbf{M}^i \mathbf{B}^i \quad (6.3)$$

$$\boldsymbol{\kappa}^i = \mathbf{B}^{iT} \mathbf{K}^i \mathbf{B}^i \quad (6.4)$$

where \mathbf{M}^i and \mathbf{K}^i are the mass and stiffness matrices of component i in component physical co-ordinates \mathbf{u} , $\boldsymbol{\mu}^{(i)}$ and $\boldsymbol{\kappa}^{(i)}$ are the mass and stiffness matrices of component i in component modal coordinates and

$$\mathbf{q} = \begin{bmatrix} \mathbf{q}_k^{(1)} \\ \mathbf{q}_c^{(1)} \\ \mathbf{q}_k^{(2)} \\ \mathbf{q}_c^{(2)} \end{bmatrix} \quad (6.5)$$

where $\mathbf{q}_k^{(i)}$ are the component modal coordinates and $\mathbf{q}_c^{(i)}$ are the constraint co-ordinates for the i th component. To assemble the component modal matrices for components 1 and 2 using \mathbf{K}_{MPC} , the component modal co-ordinates \mathbf{q} are transformed into linearly independent component modal co-ordinates \mathbf{v} using a transformation matrix \mathbf{S} that relates all the component modal coordinates as

$$\mathbf{q} = \mathbf{S}\mathbf{v} \quad (6.6)$$

where

$$\mathbf{s} = \begin{bmatrix} \mathbf{I} & 0 & 0 & 0 \\ 0 & 0 & \mathbf{I} & 0 \\ 0 & \mathbf{I} & 0 & 0 \\ 0 & 0 & 0 & \mathbf{I} \end{bmatrix} \quad (6.7)$$

and

$$\mathbf{v} = \begin{bmatrix} \mathbf{q}_k^{(1)} \\ \mathbf{q}_k^{(2)} \\ \mathbf{q}_c^{(1)} \\ \mathbf{q}_c^{(2)} \end{bmatrix} \quad (6.8)$$

Here it can be noted that the constraint co-ordinates are related to the DOFs $\boldsymbol{\Delta}^{(i)}$ from equation (3.6) as

$$\begin{bmatrix} \Delta^{(1)} \\ \Delta^{(2)} \end{bmatrix} = \begin{bmatrix} \mathbf{q}_c^{(1)} \\ \mathbf{q}_c^{(2)} \end{bmatrix} = \begin{bmatrix} \mathbf{u}_c^{(1)} \\ \mathbf{u}_c^{(2)} \end{bmatrix} \quad (6.9)$$

The global mass and stiffness in the global co-ordinates \mathbf{v} are given by,

$$\mathbf{M}_R = \mathbf{S}^T \begin{bmatrix} \mu^{(1)} & 0 \\ 0 & \mu^{(2)} \end{bmatrix} \mathbf{S} \quad \text{and} \quad \mathbf{K}_R = \mathbf{S}^T \begin{bmatrix} \kappa^{(1)} & 0 \\ 0 & \kappa^{(2)} \end{bmatrix} \mathbf{S} \quad (6.10)$$

resulting in

$$\mathbf{M}_R = \begin{bmatrix} \mathbf{I}_{kk}^{(1)} & 0 & \mathbf{m}_{kc}^{(1)} & 0 \\ 0 & \mathbf{I}_{kk}^{(2)} & 0 & \mathbf{m}_{kc}^{(2)} \\ \mathbf{m}_{kc}^{(1)T} & 0 & \mathbf{m}_{cc}^{(1)} & 0 \\ 0 & \mathbf{m}_{kc}^{(2)T} & 0 & \mathbf{m}_{cc}^{(2)} \end{bmatrix} \quad \text{and} \quad \mathbf{K}_R = \begin{bmatrix} \Lambda_{kk}^{(1)} & 0 & 0 & 0 \\ 0 & \Lambda_{kk}^{(2)} & 0 & 0 \\ 0 & 0 & \mathbf{k}_{cc}^{(1)} & 0 \\ 0 & 0 & 0 & \mathbf{k}_{cc}^{(2)} \end{bmatrix} \quad (6.11)$$

where $\Lambda_{kk}^{(1)}$ and $\Lambda_{kk}^{(2)}$ are diagonal matrices of eigenvalues of component 1 and component 2 respectively. Finally the elastic connection \mathbf{K}_{MPC} can be added to the system stiffness matrices using equations (3.6), (6.9) and (6.11) as

$$\mathbf{K}_R = \begin{bmatrix} \Lambda_{kk}^{(1)} & 0 & 0 & 0 \\ 0 & \Lambda_{kk}^{(2)} & 0 & 0 \\ 0 & 0 & \mathbf{k}_{cc}^{(1)} + \mathbf{K}_{MPC}^{(11)} & \mathbf{K}_{MPC}^{(12)} \\ 0 & 0 & \mathbf{K}_{MPC}^{(21)} & \mathbf{k}_{cc}^{(2)} + \mathbf{K}_{MPC}^{(22)} \end{bmatrix} \quad (6.12)$$

It can be observed that if the location of the point connection changes within the element, only the terms in the matrix \mathbf{K}_{MPC} change. This means that to obtain the reduced mass and stiffness matrices \mathbf{M}_R and \mathbf{K}_R when the location of the point connection changes, only the matrix \mathbf{G} in equation (3.1) needs to be re-calculated and equation (3.4) re-evaluated, offering a reduction in computation time.

6.1 Frequency response function

The equation of motion for forced vibrations in co-ordinates \mathbf{v} is given by

$$\mathbf{M}_R \ddot{\mathbf{v}} + \mathbf{K}_R \mathbf{v} = \mathbf{f}_{(v)} \quad (6.13)$$

If harmonic motion is assumed, $\mathbf{v} = \mathbf{V}e^{i\omega t}$ and $\mathbf{f}_{(v)} = \mathbf{F}_{(v)}e^{i\omega t}$ then

$$\mathbf{V} = [\mathbf{K}_R - \omega^2 \mathbf{M}_R]^{-1} \mathbf{F}_{(v)} \quad (6.14)$$

The transformation from linearly independent modal co-ordinates \mathbf{v} to the physical component \mathbf{u} co-ordinates is given by equations (6.6) and (6.2) as

$$\mathbf{U} = \mathbf{B}\mathbf{S}\mathbf{V} \quad (6.15)$$

One can express the modal forces $\mathbf{F}_{(v)}$ in terms of the specified actual forces $\mathbf{F}_{(u)}$

$$\mathbf{F}_{(v)} = \mathbf{S}^T \mathbf{B}^T \mathbf{F}_{(u)} \quad (6.16)$$

Then in physical co-ordinates the receptance matrix \mathbf{A} is given by

$$\mathbf{A} = \mathbf{B}\mathbf{S} [\mathbf{K}_R - \omega^2 \mathbf{M}_R]^{-1} \mathbf{S}^T \mathbf{B}^T \quad (6.17)$$

Finally, the response at nodal point r with an excitation of unit amplitude at nodal point e is given by the term $\mathbf{A}(r, e)$ in the \mathbf{A} matrix. Introducing damping with a loss factor η , this can be evaluated using the matrix product

$$A_{r,e} = \mathbf{B}^{r*} \mathbf{S} [\mathbf{K}_R (1 + i\eta) - \omega^2 \mathbf{M}_R]^{-1} \mathbf{S}^T \mathbf{B}^{e*T} \quad (6.18)$$

where \mathbf{B}^{r*} and \mathbf{B}^{e*} are the r^{th} and e^{th} row of \mathbf{B} respectively. The method outlined here is validated in the following section.

6.2 Numerical validation

The numerical example is the same system as used in section 5.3. Using MPCs, the elastic connection is located at the midpoint of the element that surrounds the area in which the position varies, represented as the shaded elements in Figure 10.

Using this position, the transfer mobility from coordinate (0.38, 0.32) in plate 1 to coordinate (0.38, 0.32) in plate 2 as shown in Figure 10 was evaluated. For the CMS approximation, only the first 50 modes of component 1 and the first 14 modes of component 2 were kept. Less modes of component 2 are required, because it is stiffer with fewer modes in the bandwidth considered.

The results are compared to the full FE solution in Figures 18(a) and 18(b). It is observed that the CMS approximation gives accurate results, especially below 1000Hz, saving nearly 90% of the computational time.

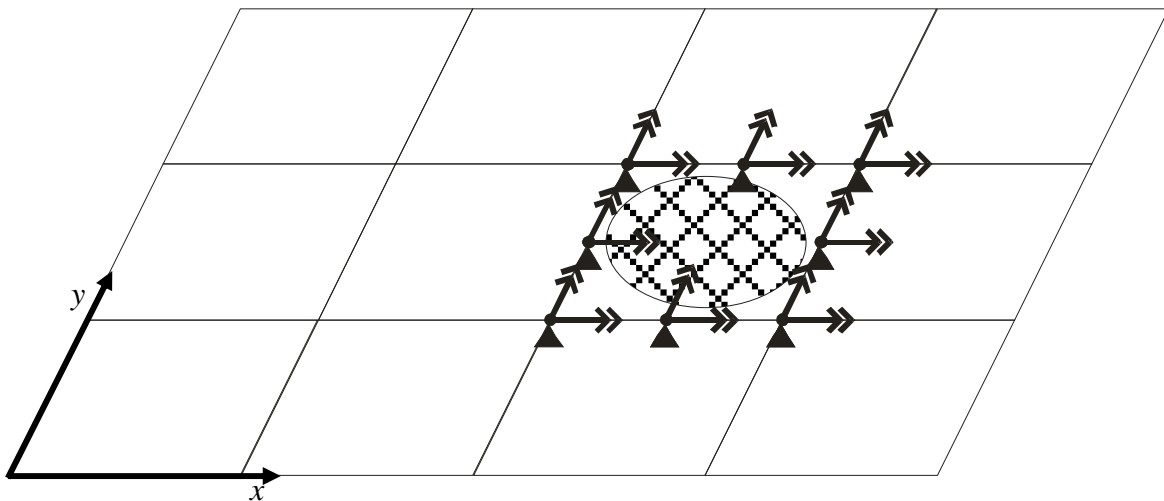


Figure 17: Constrained interface DOFs to apply CMS with MPC joints.

▣ Joint location variation, ▲ w constraint, \Rightarrow θ_x constraint, \nearrow θ_y constraint.

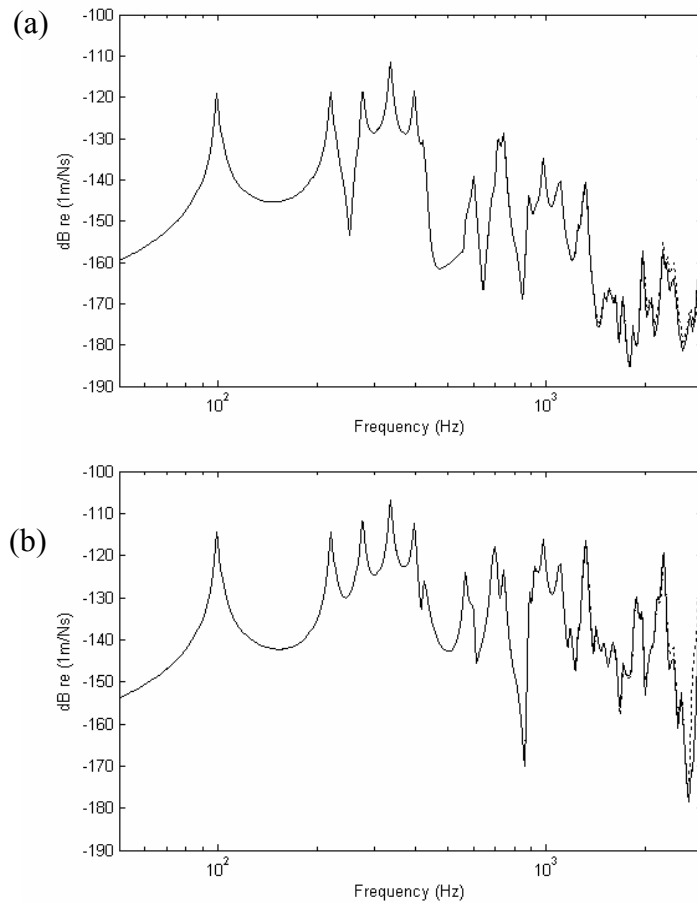


Figure 18: Transfer mobility: (a) translational stiffness connection and (b) rotational stiffness connection: ——— full solution+node to node; - - - - - CMS+MPC.

When the component mode matrix \mathbf{B} is assembled using equation (6.1), fewer modes can be kept in order to further reduce the DOFs of the system and reduce computational time. When more modes are truncated, the frequency range in which the solution is accurate is reduced i.e. the accuracy at higher frequencies is lost but the accuracy at lower frequencies is maintained.

Therefore depending on the frequency range of interest the computational efficiency can be further improved. In this example a CMS solution with 25 kept modes for the first component and 7 for the second (half the modes than the ones considered in the original CMS solution) are necessary to obtain good accuracy up to 10^3 Hz, as can be observed in Figure 19.

In Figure 19 it also can be observed how the frequency range in which the CMS solution is reduced as the number of kept modes is reduced.

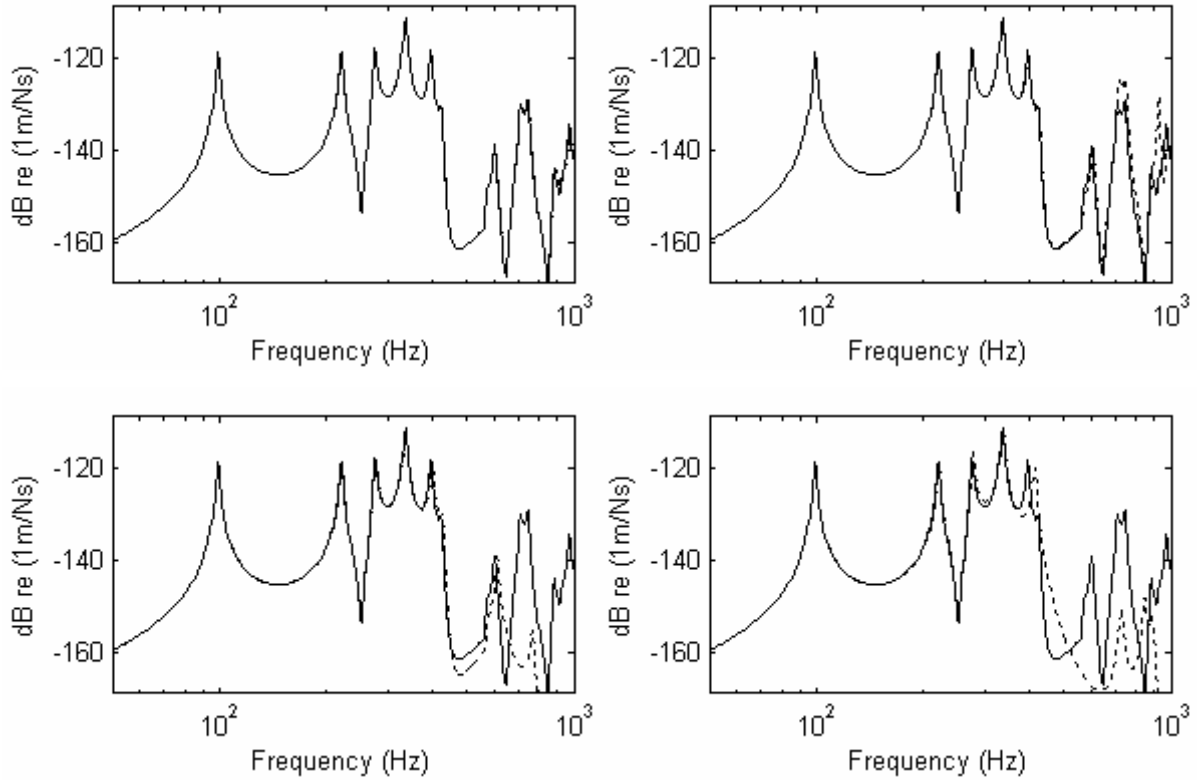


Figure 19: Transfer mobility at baseline position with a translational stiffness connection:
 — full solution; - - - - CMS:
 (a) 25 + 7 kept modes; (b) 12 + 3 kept modes; (c) 6 + 2 kept modes; (d) 3+1 kept modes

If the frequency range of interest were up to 250 Hz, keeping only 3 modes of the upper plate and 1 of the lower plate is enough to have accurate results.

To evaluate the relative stiffness of the connection, the static stiffness of the spring is compared to the sum of the point dynamic stiffness of infinite plates with the material properties and thickness of each connected plate, i.e.

$$D_{(\infty)}(\omega) = i\omega 8\sqrt{\rho h B'} \quad (6.19)$$

where ρ is the density, h is the thickness and B' is the bending stiffness of plate given by

$$B' = \frac{Eh^3}{12(1-\nu^2)} \quad (6.20)$$

where E is the Young's modulus and ν is the Poisson ratio.

For the previous numerical example, when the static stiffness of the connection $K_w = 16000 \text{ N/m}$ is compared to the sum of the magnitude of the dynamic stiffness of the connected plates at 50 Hz, $D_{(\infty)}^{1+2} = 1.36 \times 10^7 \text{ N/m}$, it can be observed that $K_w \ll D_{(\infty)}^{1+2}$.

To validate the model for different coupling conditions, the CMS+MPC model is compared to the full solution of the node to node connection model using different stiffness values: (a) $K_w < D_{(\infty)}^{1+2}$, (b) $K_w \approx D_{(\infty)}^{1+2}$ and (c) $K_w \gg D_{(\infty)}^{1+2}$. The CMS solution with 25 kept modes for the upper plate and 7 kept modes for the lower plate was seen to give accurate results up to 10^3 Hz.

For different connection stiffness values, the CMS+MPC model has a good agreement with the node to node connection and full solution as can be observed in Figure 20.

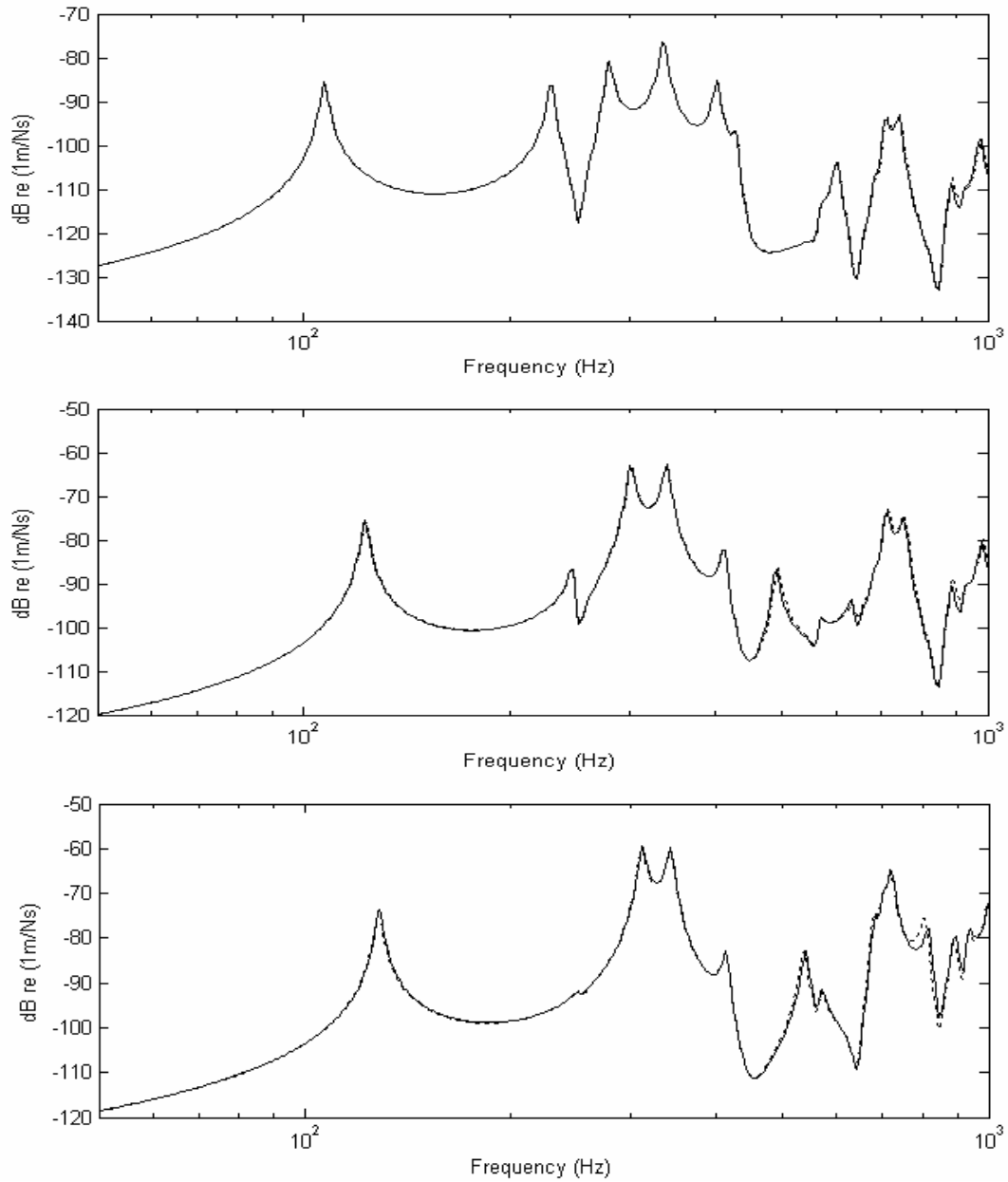


Figure 20: Transfer mobility at baseline position with a translational stiffness connection:
 — full solution, node to node; - - - - CMS+MPC:
 (a) $K_w = 10^6$; (b) $K_w = 10^7$; (c) $K_w = 10^8$

7 CONCLUSIONS

In this work multipoint constraints (MPC) were used to apply connections between structures. It was shown that an MPC connection can be placed between nodes of an FE model and is able to model the change in the location of the elastic connection in an accurate way.

When beams are connected, results showed that the MPC connection has the same performance compared to the direct node to node connections, both models giving accurate results for point connections comprising a translational or rotational spring.

Results showed that the MPC connection is not accurate when thin plate elements are used, due to the non-conforming formulation. In contrast, when the heterosis element was used the results showed that the MPC connection is as accurate as the node-to-node connection. Additional errors appear when rotational springs are used in the connection, due to discrepancies between the element formulation and the analytical solution. Some convergence issues exist in the modal summation when rotational DOFs are involved; however the solution is still acceptable.

MPCs can be used to apply forces to an FE model at any location even if there is no node at the required location.

When MPC connection is applied in combination with component mode synthesis (CMS), CMS gives a sub-structuring framework and a reduction in the number of the degrees of freedom (DOF) of the model. Combining both approaches, the response of the system can be evaluated for any connection location using the unchanged modal representation of the substructures in an accurate and numerically efficient manner.

For different element size models and for different connection stiffness values, the CMS+MPC model has a good agreement with the full solution of a node to node connection model.

8 ACKNOWLEDGMENTS

Ricardo de Alba thanks CONACYT for sponsoring his Ph.D.

9 REFERENCES

- [1] M. Petyt, *Introduction to finite element vibration analysis*. 1990, Cambridge: Cambridge University Press.
- [2] L. Hinke, B.R. Mace, and T.P. Waters, *Analysis of structures with uncertain parameters using component mode synthesis*, Proceedings of ISMA 2006, paper number 1935. Leuven, Belgium
- [3] P. Lardeur, E. Lacouture, and E. Blain. *Spot weld modelling techniques and performances of finite element models for the vibrational behaviour of automotive structures*. Proceedings of ISMA 2000. Leuven, Belgium
- [4] M. Palmonella, et al., *Finite element models of spot welds in structural dynamics: review and updating*. Computers & Structures, 2005. **83**(8-9): p. 648-61.
- [5] K. Pal and D.L. Cronin, *Static and dynamic characteristics of spot welded sheet metal beams*. Journal of Engineering for Industry, Transactions of the ASME, 1995. **117**(3): p. 316-322.
- [6] C.M. Heiserer D., Sielaft J., *High Performance Process Oriented Spot Weld Approach*, in *1st MSC Worldwide Automotive User Conference*. Sept. 1999: Munich, Germany.
- [7] *MSC. Nastran*. 2004. p. User's manual
- [8] S. Donders, et al., *The effect of spot weld failure on dynamic vehicle performance*. Sound and Vibration, 2005. **39**(4): p. 16-25.
- [9] H.C. Fang J., Holman B., Mueller F., Wallerstein D., *Weld modelling with MSC.Nastran*, in *2nd MSC Worldwide Automotive User Conference*. Oct. 2000.: Dearborn, MI.
- [10] M.S. Sheppard, *Linear multipoint constraints applied via transformation as part of a direct stiffness assembly process*. International Journal for Numerical Methods in Engineering, 1984. **20**(11): p. 2107-2112.
- [11] J.F. Doyle, *Wave propagation in structures : spectral analysis using fast discrete Fourier transforms*. 2nd ed. Mechanical engineering series. 1997, New York: Springer.
- [12] W. Soedel, *Vibrations of shells and plates*. 3rd ed. Mechanical engineering. 2004, New York, Great Britain Marcel Dekker. xxiv, 553 p.
- [13] T.J.R. Hughes and M. Cohen, *The 'heterosis' finite element for plate bending*. Computers and Structures, 1978. **9**(5): p. 445-50.
- [14] H. Nguyen-Xuan, et al., *A smoothed finite element method for plate analysis*. Computer Methods in Applied Mechanics and Engineering, 2008. **197**(13-16): p. 1184-1203.
- [15] P. Shorter, *Combining finite elements and statistical energy analysis*. 1998, University of Auckland.
- [16] F. Fahy and J. Walker, *Advanced applications in acoustics, noise and vibration*. 2004, London: Spon. xiii, 640 p.
- [17] R.R. Craig, Jr. and M.C.C. Bampton *Coupling of substructures for dynamic analyses*. AIAA Journal, 1968. **6**(7): p. 1313-1319.

APPENDIX A

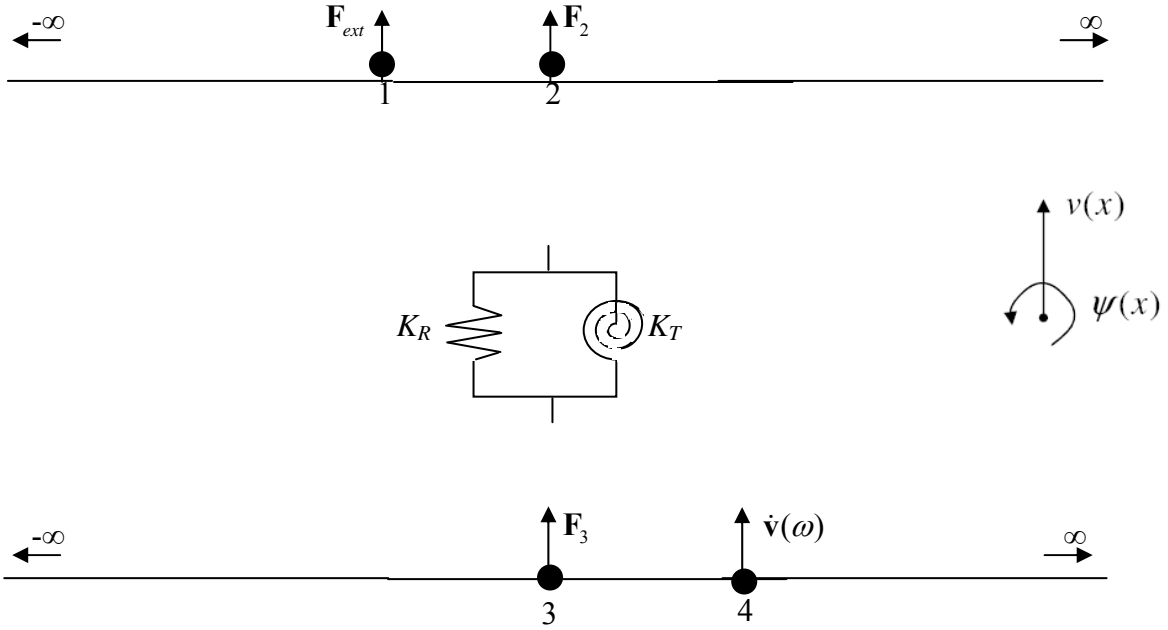


Figure A-1: Two infinite beams with a single elastic connection comprising translational and rotational stiffness

For this system each point has two degrees of freedom, therefore the forces and displacement matrixes at each node are

$$\mathbf{v}_i = \begin{bmatrix} v_i \\ \psi_i \end{bmatrix} \quad (\text{A.1})$$

$$\mathbf{F}_i = \begin{bmatrix} F_i \\ M_i \end{bmatrix} \quad (\text{A.2})$$

Then the mobility matrix \mathbf{Y}_{ij} relates the force matrix in point i and the velocity matrix in point j as

$$\dot{\mathbf{v}}_j = \mathbf{Y}_{ij} \mathbf{F}_i \quad (\text{A.3})$$

where \mathbf{Y}_{ij} containing the following elements $Y_{\dot{v},F}^{i-j} = i\omega v_j / F_i$, $Y_{\psi,F}^{i-j} = i\omega \psi_j / F_i$, $Y_{\dot{v},M}^{i-j} = i\omega v_j / M_i$ and $Y_{\psi,M}^{i-j} = i\omega \psi_j / M_i$

The equations defining the system in Figure A.1 are; for the upper beam

$$\dot{\mathbf{v}}_2 = \mathbf{Y}_{12}\mathbf{F}_{ext} + \mathbf{Y}_{22}\mathbf{F}_2 \quad (\text{A.4})$$

for the lower beam

$$\dot{\mathbf{v}}_4 = \mathbf{Y}_{34}\mathbf{F}_3 \quad (\text{A.5})$$

Finally the spring can be defined in terms of its mobility

$$\begin{bmatrix} \dot{\mathbf{v}}_2 \\ \dot{\mathbf{v}}_3 \end{bmatrix} = \mathbf{Y}_s \begin{bmatrix} \mathbf{F}_{e2} \\ \mathbf{F}_{e3} \end{bmatrix} \quad (\text{A.5})$$

here the equilibrium forces are

$$\begin{bmatrix} \mathbf{F}_{e2} \\ \mathbf{F}_{e3} \end{bmatrix} = \begin{bmatrix} -\mathbf{F}_2 \\ -\mathbf{F}_3 \end{bmatrix} \quad (\text{A.6})$$

Finally for the system in Figure A-1, the connection is massless. Therefore

$$\mathbf{F}_2 = \mathbf{F}_3 \quad (\text{A.7})$$

APPENDIX B

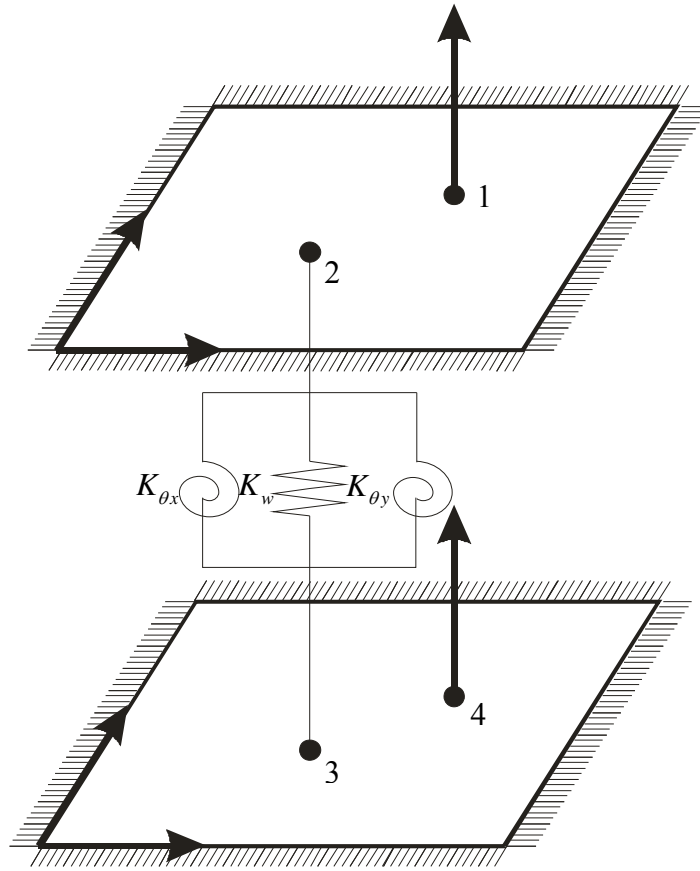


Figure B-1: Two simply supported plates with a single elastic connection comprising translational and two rotational stiffnesses

For this system each point has three degrees of freedom, therefore the forces and displacement matrixes at each node are

$$\mathbf{v}_i = \begin{bmatrix} v_i \\ \psi_{xi} \\ \psi_{yi} \end{bmatrix} \quad (\text{B.1})$$

$$\mathbf{F}_i = \begin{bmatrix} F_i \\ M_{xi} \\ M_{yi} \end{bmatrix} \quad (\text{B.2})$$

Then the mobility matrix \mathbf{Y}_{ij} relates the force matrix in point i and the velocity matrix in point j as

$$\dot{\mathbf{v}}_j = \mathbf{Y}_{ij} \mathbf{F}_i \quad (\text{B.3})$$

where \mathbf{Y}_{ij} containing the following elements $Y_{\dot{v},F}^{i-j} = i\omega v_j / F_i$, $Y_{\dot{\psi},F}^{i-j} = i\omega \psi_{xj} / F_i$,
 $Y_{\dot{\psi},F}^{i-j} = i\omega \psi_{yj} / F_i$, $Y_{\dot{v},Mx}^{i-j} = i\omega v_j / M_{xi}$, $Y_{\dot{\psi},Mx}^{i-j} = i\omega \psi_{xj} / M_{xi}$, $Y_{\dot{\psi},Mx}^{i-j} = i\omega \psi_{yj} / M_{xi}$, $Y_{\dot{v},My}^{i-j} = i\omega v_j / M_{yi}$,
 $Y_{\dot{\psi},My}^{i-j} = i\omega \psi_{xj} / M_{yi}$ and $Y_{\dot{\psi},My}^{i-j} = i\omega \psi_{yj} / M_{yi}$.

The equations defining the system in Figure B.1 are; for the upper plate

$$\dot{\mathbf{v}}_2 = \mathbf{Y}_{12} \mathbf{F}_{ext} + \mathbf{Y}_{22} \mathbf{F}_2 \quad (\text{B.4})$$

for the lower plate

$$\dot{\mathbf{v}}_4 = \mathbf{Y}_{34} \mathbf{F}_3 \quad (\text{B.5})$$

Finally the spring can be defined in terms of its mobility

$$\begin{bmatrix} \dot{\mathbf{v}}_2 \\ \dot{\mathbf{v}}_3 \end{bmatrix} = \mathbf{Y}_s \begin{bmatrix} \mathbf{F}_{e2} \\ \mathbf{F}_{e3} \end{bmatrix} \quad (\text{B.5})$$

here the equilibrium forces are

$$\begin{bmatrix} \mathbf{F}_{e2} \\ \mathbf{F}_{e3} \end{bmatrix} = \begin{bmatrix} -\mathbf{F}_2 \\ -\mathbf{F}_3 \end{bmatrix} \quad (\text{B.6})$$

Finally for the system in Figure B-1, the connection is massless. Therefore

$$\mathbf{F}_2 = \mathbf{F}_3 \quad (\text{B.7})$$